2-11-2020

Prebiotic-Induced Anti-tumor Immunity Attenuates Tumor Growth

Yan Li

Lisa Elmen

Igor Segota

Yibo Xian

Roberto Tinoco

See next page for additional authors

Authors

Yan Li, Lisa Elmen, Igor Segota, Yibo Xian, Roberto Tinoco, Tinoco Feng, Yu Fujita, Rafael R. Segura Munoz, Robert J. Schmaltz, Linda M. Bradley, Amanda Ramer-Tait, Raphy Zarecki, Tao Long, Scott N. Peterson, and Ze'ev A. Ronai

Prebiotic-Induced Anti-tumor Immunity Attenuates Tumor Growth

Graphical Abstract

Highlights

- Mucin and inulin, prebiotics, inhibit melanoma growth in syngeneic mouse models

- Changes in gut microbiota taxa by these prebiotics induce anti-tumor immunity

- Inulin attenuates melanoma resistance to MEKi in a mouse melanoma model

- Inulin and mucin elicit distinct microbiota changes and an additive effect in select models
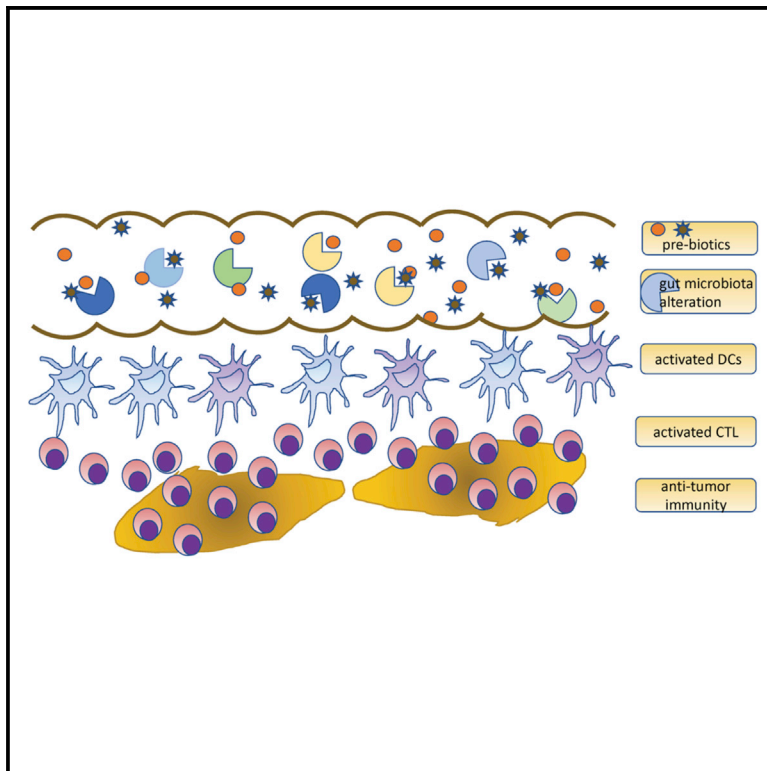
Authors

Yan Li, Lisa Elmén, Igor Segota, ...,
Tao Long, Scott N. Peterson,
Ze'ev A. Ronai

Correspondence

speterson@sbpdiscovery.org (S.N.P.),
zeev@ronailab.net (Z.A.R.)

In Brief

Li et al. show that the gut microbiota effect on anti-tumor immunity is affected by inulin or mucin, prebiotics that inhibit melanoma and colon cancer growth in syngeneic models and attenuate melanoma resistance to MEKi. These studies highlight a potential therapeutic role for prebiotics in shaping the microbiota composition to promote anti-tumor immunity.

Prebiotic-Induced Anti-tumor Immunity Attenuates Tumor Growth

Yan Li,[1] Lisa Elmén,[1,5] Igor Segota,[1,5] Yibo Xian,[2] Roberto Tinoco,[1,4] Yongmei Feng,[1] Yu Fujita,[1] Rafael R. Segura Muñoz,[2] Robert Schmaltz,[2] Linda M. Bradley,[1] Amanda Ramer-Tait,[2] Raphy Zarecki,[3] Tao Long,[1] Scott N. Peterson,[1,*] and Ze'ev A. Ronai[1,6,*]

[1]Sanford Burnham Prebys Medical Discovery Institute, La Jolla, CA 92037, USA
[2]Department of Food Science and Technology, University of Nebraska-Lincoln, Lincoln, NE 68588, USA
[3]Technion Integrated Cancer Center, Faculty of Medicine, Technion, Haifa 3525433, Israel
[4]Present address: Department of Molecular Biology and Biochemistry, University of California, Irvine, Irvine, CA 92697, USA
[5]These authors contributed equally
[6]Lead Contact
*Correspondence: speterson@sbpdiscovery.org (S.N.P.), zeev@ronailab.net (Z.A.R.)
 https://doi.org/10.1016/j.celrep.2020.01.035

SUMMARY

Growing evidence supports the importance of gut microbiota in the control of tumor growth and response to therapy. Here, we select prebiotics that can enrich bacterial taxa that promote anti-tumor immunity. Addition of the prebiotics inulin or mucin to the diet of C57BL/6 mice induces anti-tumor immune responses and inhibition of BRAF mutant melanoma growth in a subcutaneously implanted syngeneic mouse model. Mucin fails to inhibit tumor growth in germ-free mice, indicating that the gut microbiota is required for the activation of the anti-tumor immune response. Inulin and mucin drive distinct changes in the microbiota, as inulin, but not mucin, limits tumor growth in syngeneic mouse models of colon cancer and NRAS mutant melanoma and enhances the efficacy of a MEK inhibitor against melanoma while delaying the emergence of drug resistance. We highlight the importance of gut microbiota in anti-tumor immunity and the potential therapeutic role for prebiotics in this process.

INTRODUCTION

Melanoma remains one of the most aggressive tumor types, mainly because of its propensity to metastasize and resist therapy. Aberrant activation of the mitogen-activated protein kinase (MAPK) pathway has been reported in human BRAF and NRAS mutant tumors, including melanomas, in which they account for more than 70% of genetic changes. Although selective inhibitors to BRAF mutant proteins have been developed, their effectiveness is limited by the frequent emergence of resistance (Brighton et al., 2018; Fedele et al., 2018; Martz et al., 2014). Inhibitors of the MAPK pathway, including MEK, have also been developed and are commonly used for the treatment of NRAS mutant melanomas (Johnson and Puzanov, 2015). The emergence of immune checkpoint therapy

has resulted in unprecedented clinical success and offered new therapeutic modalities (Colli et al., 2017; Eggermont et al., 2018; Ribas et al., 2019). At present, BRAF inhibitors (BRAFi) and MEK inhibitors (MEKi) are being tested in several clinical trials, in combination with other therapies, including immune checkpoint inhibitors and gut microbiota modulators (Humphries and Daud, 2018; Matson et al., 2018; York, 2018).

The gastrointestinal (GI) tract harbors a complex and dynamic population of bacteria, called gut microbiota, that are implicated in the maintenance of health and the onset and progression of disease (Sommer and Bäckhed, 2013). In these roles, gut microbiota affect key components of host physiology and homeostasis, including the development and function of the immune system (Bäckhed et al., 2005; Ley et al., 2008). Changes in gut microbiota composition are linked to local and systemic alterations that affect tumor growth, in part through modulation of tissue remodeling, mucosal immunity, and anti-tumor immunity (Rutkowski et al., 2015). Gut microbiota also influence the incidence and progression of colorectal carcinoma (Arthur et al., 2012; Bonnet et al., 2014) and breast and hepatocellular carcinoma (Arthur et al., 2012; Dapito et al., 2012). The importance of gut microbiota composition in cancer (Adolph et al., 2013) has been further demonstrated in studies showing the ability of the microbiota to enhance responses to checkpoint inhibitors such as anti-PD-(L)1 antibodies (Gopalakrishnan et al., 2018b; Haapanen et al., 1997; Matson et al., 2018; Sivan et al., 2015) and anti-CTLA-4 antibodies (Chaput et al., 2017; Vétizou et al., 2015). Furthermore, bacterial commensals that were found to be more abundant in the gut of melanoma patients responding to anti-PD-1 therapy (Gopalakrishnan et al., 2018b; Haapanen et al., 1997; Matson et al., 2018; Sivan et al., 2015), provided a rationale for performing fecal microbiota transplantation to non-responding patients.

Despite their clinical efficacy, checkpoint inhibitors are effective in only a fraction of treated patients. Human fecal microbiota derived from therapy-responsive patients confer treatment responsiveness when transplanted into germ-free (GF) mice (Matson et al., 2018; Routy et al., 2018), while a small set of phylogenetically unrelated gut microbiota species

was suggested to promote anti-tumor phenotypes. For example, introduction of *Bacteroides thetaiotaomicron* or *Bacteroides fragili* to GF mice was sufficient to restore anti-tumor responses via induction of a skewed T_h1 response (Vétizou et al., 2015). Our recent study demonstrated that *Bacteroides rodentium* induced anti-tumor immunity in melanoma and colon cancer models that were subcutaneously implanted in syngeneic C57BL/6 mice (Li et al., 2019b). In another study, the abundance of *Akkermansia muciniphila* was associated with anti-PD-1 responsiveness in humans and restored an anti-tumor phenotype when co-administered with anti-PD-1 therapy to melanoma patients (Routy et al., 2018). Administration of *Bifidobacterium* spp. in combination with anti-PD-L1 agents, attenuated tumor growth and promoted anti-tumor immunity in a syngeneic mouse model (Sivan et al., 2015). Moreover, human melanoma patients who responded to anti-CTLA-4 (ipilimumab) were found to have gut microbiota enriched in three butyrate-producing bacterial species (Chaput et al., 2017), and administration of *Enterococcus hirae* and *Barnesiella intestinihominis* improved their response to cyclophosphamide chemotherapy (Daillère et al., 2016). An assessment of mice treated with various antibiotics revealed that ampicillin-treated mice retained a simplified microbiota with a potent anti-tumor phenotype (Tanoue et al., 2019). Isolates from these mice identified 11 strains, enriched in *Bacteroides*, *Parabacteroides*, *Alistipes*, and an uncharacterized Ruminococcaceae, that increased the abundance of CD8$^+$ interferon-γ (IFN-γ)-producing cells in the gut and potentiated anti-PD-1- and anti-CTLA-4-mediated control of tumor growth. Collectively, these findings point to the importance of gut microbiota in controlling cancer growth and reveal the complex variety of species that can promote anti-tumor immunity.

Previous reports indicated that the prebiotic inulin increases the relative abundance of *Bifidobacteria*, *Bacteroides*, and *Akkermansia muciniphila* in mice (Everard et al., 2013; Fehlbaum et al., 2018; Li et al., 2019a; Singh et al., 2018). Among these, *Akkermansia muciniphila* is known to reside in the mucin layer of the GI tract, in which it consumes glycan substrates decorating mucin proteins (muc2). Our earlier studies identified microbiota-dependent anti-melanoma immunity in syngeneic *Rnf5*$^{-/-}$ mice, which was conferred by select bacterial strains that induced tumor infiltration by T cells and dendritic cells (DCs) and inhibited melanoma growth upon their inoculation in GF mice (Li et al., 2019b).

The prebiotics inulin and mucin have been reported to induce *Bifidobacterium* spp. and *Akkermansia muciniphila* (Everard et al., 2013; Fehlbaum et al., 2018; Li et al., 2019a; Singh et al., 2018). Cultivation of fecal samples with inulin and mucin increased the relative abundance of several species implicated in tumor growth control in the *Rnf5*$^{-/-}$ mice (Li et al., 2019b). Therefore, in this study, we investigated the effects of inulin and porcine gastric mucin on growth of a subcutaneously implanted tumor and its propensity to resist targeted therapy in syngeneic mouse models. We demonstrate the ability of these prebiotics to elicit changes in gut microbiota composition that play a pivotal role in eliciting effective anti-tumor immunity.

RESULTS

Prebiotic Treatment of Fecal Microbiota *In Vitro* Enriches for Taxa that Promote Anti-tumor Immunity

Inulin and mucin have been shown to alter the relative abundance of bacterial species that were identified as anti-tumor immunity-promoting bacteria in *Rnf5*$^{-/-}$ mice, including *Parasutterella excrementihominis*, *Bacteroides rodentium*, and *Clostridium viride* (Figures S1A and S1B). We thus tested the effect of inulin and mucin on anaerobic cultivation of 12 fecal samples derived from healthy human subjects. Both prebiotics increased the relative abundance of *Bacteroides* spp., whereas only mucin increased the relative abundance of *Akkermansia muciniphila* in most cultures (Figure S1C). Surprisingly, inulin, but not mucin, promoted the growth of *Bifidobacteria* spp. in only two of the cultures.

Feeding of Mucin or Inulin to Wild-Type Mice Reduces Tumor Growth and Induces Anti-tumor Immunity

Inulin is a naturally occurring fructosyl polymer with chain-terminating glucosyl residues. Mucins are highly decorated with polysaccharides composed of various core structures similar to those found in Lewis blood type antigens, including the sugars galactose, fucose, sialic acid, galactosamine, glucosamine, and mannose. To determine whether prebiotics inhibit tumor growth, mucin (3% in drinking water) or inulin (15% w/w in chow) were administered to wild-type (WT) C57BL/6 mice starting 2 weeks before subcutaneous injection of syngeneic melanoma tumor cells (YUMM1.5 cells, 1×10^6 cells/mouse) through the remainder of the experiment. Administration of mucin or inulin led to attenuated melanoma tumor growth (Figure 1A). To determine whether these changes could be attributed to anti-tumor immunity, we analyzed tumor-infiltrating lymphocytes (TILs) 20 days following tumor inoculation. Compared with control mice, tumors from mucin- or inulin-treated mice were enriched in CD45$^+$ cells, including effector (CD44^{hi}) CD4$^+$ and CD8$^+$ T cells (e.g., IFN-γ-producing CD4$^+$ T cells), plasmacytoid DCs, and conventional CD8α^+ DCs (Figures 1B–1D). Tumor-resident DCs isolated from inulin- or mucin-treated C57BL/6 mice expressed higher levels of major histocompatibility complex (MHC) class I and MHC class II (Figure 1E), implying greater stimulatory capacity, compared with the tumor-associated cells from control mice. These data indicate that prebiotic supplementation induced a shift to a proinflammatory tumor microenvironment associated with a more potent anti-tumor response. The immunomodulatory effects of the two prebiotics were largely overlapping, but not identical, yet had similar effects on tumor control. Antibody-mediated depletion of CD4$^+$ and CD8$^+$ T cells in inulin-treated mice (Figure 1F) reduced the suppression of tumor growth, pointing to an essential role for CD4$^+$ and CD8$^+$ T cells in the inulin-promoted anti-tumor phenotype.

Mucin and Inulin Feeding Enhances Expression of Anti-tumor Immunoregulatory Genes in Tumors

To identify possible mechanisms for the elevated immune cell infiltration and anti-tumor immunity in prebiotic-treated mice, we examined tumor-xenograft samples grown in syngeneic
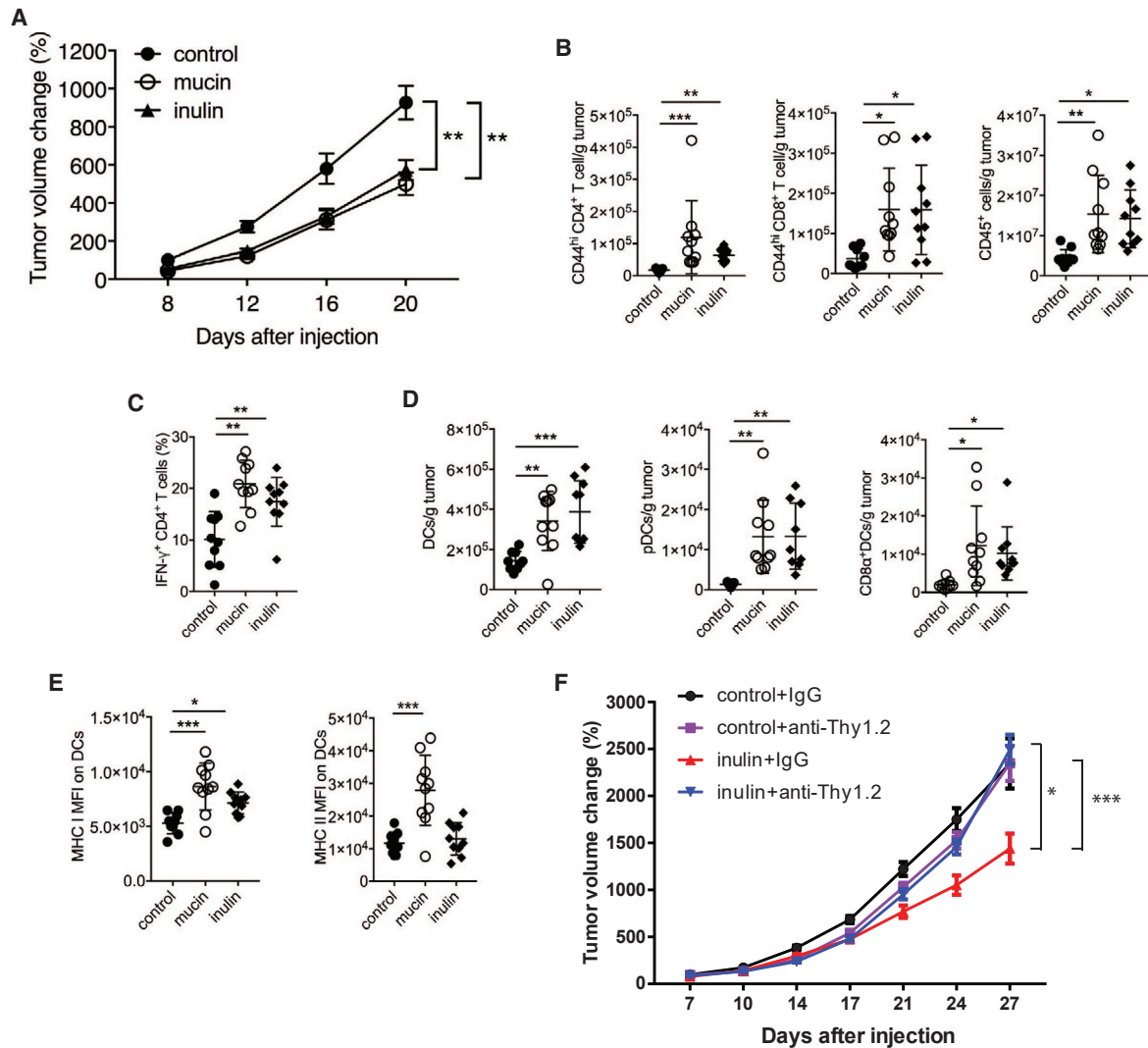
Figure 1. Administration of Mucin or Inulin Reduces Tumor Growth and Induces Anti-tumor Immunity

(A) Growth of YUMM1.5 tumors that were subcutaneously transplanted in syngeneic C57BL/6 mice. Mice were provided with a control diet, 3% mucin in drinking water, or 15% inulin-supplemented chow starting 14 days before tumor inoculation (control, n = 12; mucin, n = 15; inulin, n = 15).

(B) Quantification of tumor-infiltrating total CD45^{+} cells and effector (CD44^{hi}) CD4^{+} or CD8^{+} T cells from mice treated as in (A) (control, n = 9; mucin, n = 10; inulin, n = 10).

(C) Quantification of tumor-infiltrating, IFN-γ-producing CD4^{+} T cells from mice treated as in (A) (n = 10).

(D) Quantification of tumor-infiltrating total DCs and DC subsets in mice treated as in (A) (control, n = 9; mucin, n = 10; inulin, n = 10).

(E) MFI of MHC class I and MHC class II on tumor-infiltrating DCs in mice treated as in (A) (control, n = 9; mucin, n = 10; inulin, n = 10).

(F) Wild-type C57BL/6 mice (n = 12) were fed control or 15% inulin-supplemented chow starting 14 days before subcutaneous (s.c.) injection of YUMM1.5 melanoma cells (1 × 10^{6}). Anti-mouse Thy1.2 or control immunoglobulin G (IgG, 400 μg) were injected two times a week starting 3 days after tumor inoculation (n = 12). Tumor volume was assessed two times a week. FACS analysis revealed >90% depletion of blood CD4^{+} and CD8^{+} T cells on day 8 after tumor inoculation. Data are representative of three independent experiments (A–E) or one experiment (F). Graphs show the mean ± SEM. *p < 0.05, **p < 0.005, ***p < 0.001, ****p < 0.0001 by two-way ANOVA with Bonferroni's correction (A and F) or by one-way ANOVA with Bonferroni's correction (B–E).

mouse models for changes in the transcription of immune-associated genes (including chemokines), inflammasome activity, and antigen presentation. Both prebiotics increased the expression of chemokines (CCL4 and CCL8), inflammasome-related genes (TLR3 and TLR7), and antigen presentation-related genes (CD40, Stat1, and ICOS) (Figure 2A), suggesting a mechanism by which prebiotic supplementation enhanced

the recruitment and activation of immune cells in the tumor microenvironment.

Independent support for the activation of T cells in prebiotic-treated mice was obtained using the OVA-specific OT-I transgenic mouse model. WT OT-I CD8^{+} CD45.1^{+} T cells were transferred to untreated or mucin-treated WT mice harboring B16F10-OVA melanoma tumors, and their frequency in tumor-draining and
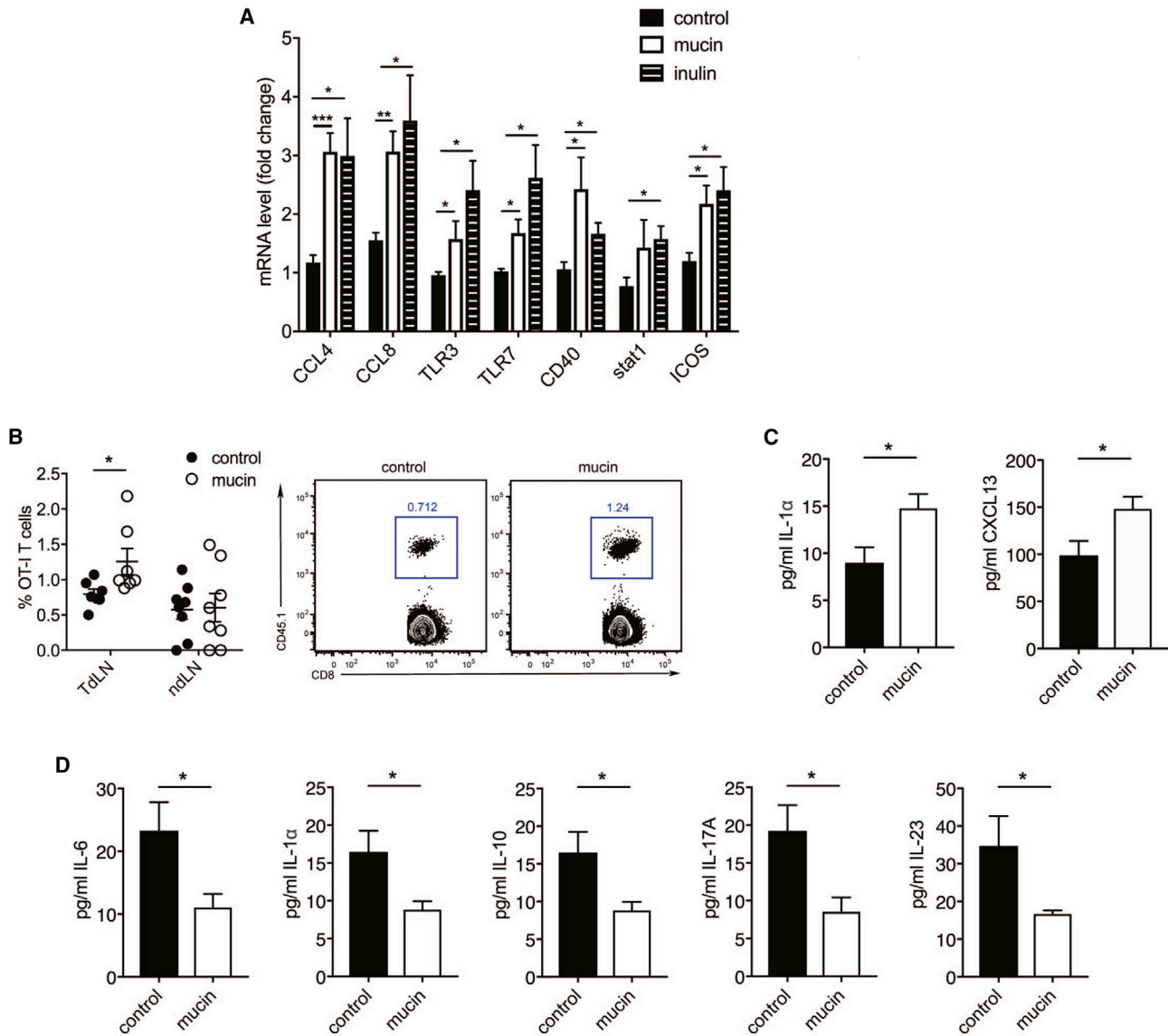
Figure 2. Mucin and Inulin Induce Enhanced Expression of Immunoregulatory Genes in Tumors

(A) qPCR analysis of immune-related genes in subcutaneously transplanted melanoma grown in syngeneic C57BL/6 mice that received a control diet, 3% mucin in drinking water, or 15% inulin-supplemented chow starting 14 days before tumor inoculation (n = 6).

(B) Quantification of CD45.1^{+} OT-I CD8^{+} T cells in the tumor-draining lymph nodes (TdLN) and non-draining lymph nodes (ndLN) of C57BL/6 mice (CD45.2^{+}) treated with or without mucin and injected with B16-OVA melanoma cells (TdLN, n = 7; ndLN, n = 8). Right dot plots show gating of CD45.1^{+} CD8^{+} cells.

(C) Serum cytokine and chemokine levels in naive WT mice treated with or without mucin (n = 10).

(D) Serum cytokines in WT mice treated with or without mucin on day 10 after tumor inoculation (n = 10).

Data are representative of three independent experiments (A and B) or one experiment (C and D). Graphs show the mean ± SEM. *p < 0.05, **p < 0.005, ***p < 0.001, ****p < 0.0001 by one-way ANOVA with Tukey's correction (A) or by two-tailed t test or Mann-Whitney U test (B–D).

non-draining lymph nodes was monitored. OT-I CD8^{+} T cells were more abundant in the draining lymph nodes of mucin-treated mice compared with control mice (Figures 2B and S2A), pointing to either increased recruitment or increased survival of OT-1 cells in the prebiotic-treated mice. Altogether, these results confirm that prebiotic treatment promotes anti-tumor immunity via effects on both innate and adaptive immune cells.

Consistent with the elevated abundance of TILs in mucin-treated compared with control C57BL/6 mice, levels of the cyto-kine interleukin (IL)-1α and chemokine CXCL13 were increased in the sera of mucin-fed mice before tumor cell inoculation (Figure 2C), suggesting that the inflammation-promoting effects of mucin were systemic. Strikingly, we found that mucin-treated tumor-xenograft-bearing mice exhibited reduced serum levels of IL-6, IL-1α, IL-10, IL-17A, and IL-23 compared with control animals (Figure 2D). High serum levels of IL-6 and IL-17 were previously associated with poor clinical outcome (Rutkowski et al., 2015; Wang et al., 2009), whereas reduced IL-1α levels
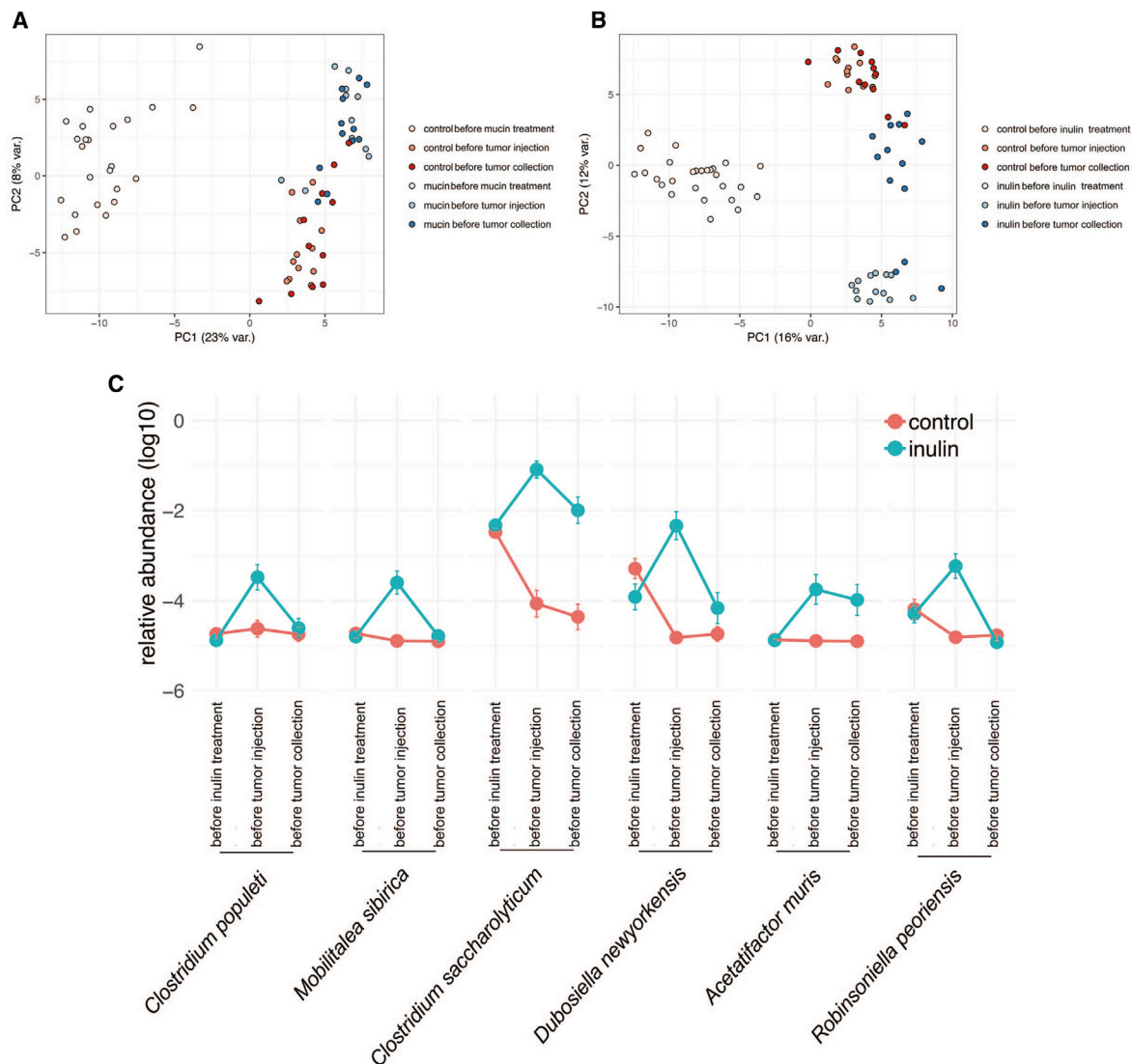
Figure 3. Mucin and Inulin Modulate the Composition and Diversity of Gut Microbiota

(A and B) Principal-component analysis of all taxa enumerated in fecal microbiota of control and mucin-treated (A) or inulin-treated (B) C57BL/6 mice, examined before prebiotic treatment, before subcutaneous injection of syngeneic YUMM1.5 tumor cells, and before tumor collection (control, n = 12; mucin, n = 15; inulin, n = 15).

(C) Time course of the relative abundance of the six taxa enriched in inulin-treated mice that negatively correlate with YUMM1.5 tumor size (control, n = 12; inulin, n = 15). Time points are before inulin treatment, before tumor injection, and before tumor collection.

Data are representative of two independent experiments.

were associated with attenuated tumor growth (Apte et al., 2006). Lower serum levels of the chemokines CXCL1 and CXCL13 were also found in mucin-treated mice compared with control mice (Figure S2B), linking levels of both chemokines and cytokines with the anti-tumor response.

Inulin and Mucin Alter Gut Microbiota

We next used 16S rRNA amplicon sequencing to profile the fecal microbiota of WT C57BL/6 mice before and 14 days after prebiotic feeding and 20 days after YUMM1.5 tumor cell inoculation, with tumor cells originally obtained from genetically engineered C57BL/6 mice harboring $Braf^{V600E}$

mutation, *Pten* deletion, and *Cdkn2a* deletion. Although the bacterial communities at baseline were heterogeneous and generally not well clustered (Figures 3A and 3B), prebiotic feeding resulted in the formation of more highly related communities that were distinct from those in control mice. Furthermore, the bacterial communities underwent additional restructuring following tumor cell inoculation. These data are consistent with recent observations that distal tumor growth results in a reconfiguration of gut microbiota (Li et al., 2019b). Individual phylotype groups (two or more highly related, but not identical, 16S sequences of strains approximating a species) that were altered in the microbiota of

control and prebiotic-treated mice were identified but were not further assessed. Thus, only phylotypes that were associated with a specific prebiotic treatment were further studied.

Sequencing of the amplified 16S V3-V4 region followed by computational analysis led to the identification of increased relative abundance of 17 phylotype groups in inulin-treated mice and 2 phylotype groups in the mucin-treated mice that were not present in control mice (Table S1). Inulin increased the relative abundance of taxa that were phylogenetically coherent, 66% of which mapped most closely to members of *Clostridium* cluster XIVa, primarily *Clostridium populeti*- and *Clostridium saccharolyticum*-related taxa (Table S1). Although this cluster consists of numerous butyrate producers, the phylogenetic distance of the phylotypes profiled here makes the butyrate-producing potential of these taxa uncertain. Among the phylotypes that displayed increased relative abundance following inulin treatment, six were negatively correlated with tumor size (Figure 3C). Mucin also predominantly enriched taxa with similarity to members of *Clostridium* cluster XIVa (Table S1); however, none of the phylotypes induced by mucin were negatively correlated with tumor size. These findings suggest that inulin and mucin drive distinct changes in gut microbiota, both of which are capable of inducing anti-tumor immunity.

Inulin Attenuates Colon Cancer Growth
We next assessed whether mucin or inulin supplementation affects the growth of tumor types other than melanoma. Using the same protocol (prebiotic feeding starting 2 weeks before tumor inoculation), we found that inulin, but not mucin, attenuated the growth of subcutaneously transplanted MC-38 colon cancer tumors in syngeneic C57BL/6 mice (Figure 4A) and enhanced the anti-tumor immune response, as reflected by increased MHC class I and MHC class II expression on DCs (Figure 4B). No differences in the abundance of CD4+ or CD8+ T cells, total CD45+ cells, DCs, or DC subsets or the production of cytokines were observed in tumors from mucin- or inulin-treated mice (Figure S3). Although both mucin and inulin induced anti-tumor immunity that limited the growth of melanoma tumors, only inulin was able to attenuate colon cancer growth. Thus, the differences in taxa induced by these prebiotics may account for their distinct effects on control of select tumor types.

Specific Microbiota Are Associated with Control of Colon Cancer Growth and Anti-tumor Immunity
Analysis of fecal microbiota from MC-38 tumor-bearing inulin- or mucin-treated mice indicated that both prebiotics increased the relative abundance of a similar number of phylotype groups (25 inulin and 21 mucin), of which 7 were common to both prebiotics (Table S2). More than 68% of the phylotype groups induced by inulin mapped to *Clostridium* cluster XIVa, compared with 33% induced by mucin. Additional analysis demonstrated that the relative abundance of six inulin-specific phylotypes was inversely correlated with MC-38 tumor size (Figure 4C), whereas no relationship with tumor size was detected for the phylotype groups induced by mucin.

Combination Treatment with Inulin Overcomes Melanoma Resistance to MEKi
We next determined whether prebiotic supplementation influenced the efficacy of MEKi treatment by examining growth of the N-RAS mutant mouse melanoma cell line MaN-RAS that was obtained from genetically engineered *N-Ras* melanoma grown in C57BL/6 mice. Syngeneic mice (C57BL/6) were subcutaneously inoculated with tumor cells 2 weeks after the initiation of feeding with inulin or mucin with or without MEKi. In the absence of MEKi, inulin, but not mucin, modestly controlled tumor growth (Figure 5A). However, co-administration of MEKi with inulin had an additive effect on tumor growth control, and the emergence of MEKi resistance was delayed compared with MEKi alone (Figure 5A), implying that MEKi resistance may be partially overcome by this prebiotic. Consistent with these findings, tumors from mice treated with inulin+MEKi contained elevated numbers of total CD45+ cells, CD4+ and CD8+ T cells, pDCs, and mDCs, and the DCs expressed elevated levels of MHC class I compared with mice treated with MEKi alone (Figures 5B and 5C). However, no differences in T cell-mediated cytokine production were detected in tumors from inulin+MEKi-treated mice (Figure S4A).

Inulin-Induced Alterations in Gut Microbiota Control NRAS Mutant Melanoma Tumor Growth and MEKi Resistance
Inulin and mucin treatment before MEKi injection increased the relative abundance of 39 and 23 phylotype groups, respectively (Figures 5D, S4B, and S4C), and the abundance of these groups was negatively correlated with tumor size (Figures S4B and S4C). Both inulin and mucin primarily increased the relative abundance of taxa mapping in or near *Clostridium* cluster XIVa (Figures 5D and 5E). Inulin specifically induced six phylotypes related to *Bacteroides* spp. (primarily *Bacteroides acidifaciens*), three phylotypes related to *Barnesiella* spp., and a group related to *Parasutterella excrementihominis*, the latter of which was not detected following mucin treatment. Inulin also increased the relative abundance of three phylotype groups related to *Bifidobacterium* spp., whereas only one group was induced by mucin. The genomes of *Bacteroides*, *Bifidobacterium*, and *Barnesiella* spp. encode numerous glycosyl hydrolase activities (http://www.cazy.org/) that support cross-feeding interactions with sugar-fermenting bacteria, particularly *Clostridiales* spp.

Mice treated with doses of MEKi alone that effectively controlled subcutaneously implanted MaN-RAS1 tumor growth in syngeneic C57BL/6 mice showed enrichment of 14 phylotype groups in the gut microbiota, none of which negatively correlated with tumor size (Table S3). Analysis of taxa in tumor-bearing mice fed inulin identified eight phylotype groups enriched in *Actinobacteria*, *Bifidobacterium longum*, and two *Olsenella* spp. (Table S3). Only one phylotype group mapping distantly to *Clostridium cellobioparum* was negatively correlated with tumor size. Mucin treatment alone resulted in an increase in the relative abundance of 56 phylotype groups featuring diversity of taxa, including *Bacteroides*, *Parabacteroides*, *Olsenella*, and *Clostridium*. Mucin uniquely increased the relative abundance of five *Lactobacillus* spp., all of which were positively correlated with tumor size, albeit not to the level of statistical significance. Mucin feeding
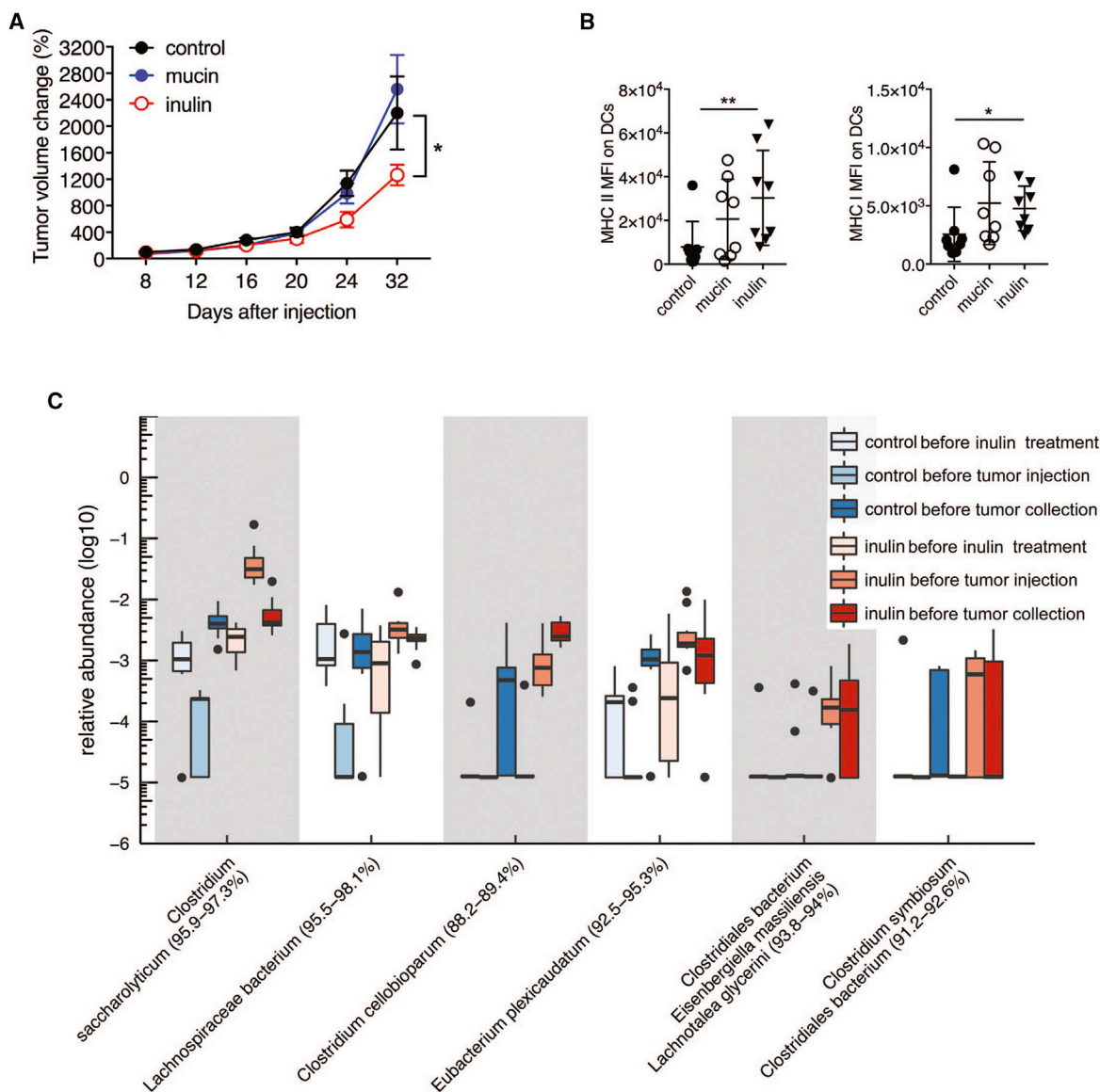
Figure 4. Inulin Controls Colon Cancer Growth and Induces Anti-tumor Immunity

(A) Growth of MC-38 mouse colorectal cancer cells (1×10^6) injected subcutaneously into syngeneic C57BL/6 mice that received control diet, 3% mucin in drinking water, or 15% inulin-supplemented chow starting 14 days before tumor inoculation (control, n = 9; mucin, n = 15; inulin, n = 15).

(B) MFI of MHC class II and MHC class I in MC-38 tumor-infiltrating DCs (n = 8).

(C) Boxplot of the relative abundance of the taxa enriched in inulin-treated mice and positively correlated with tumor size (n = 10).

Data are representative of two independent experiments. Graphs show the mean ± SEM. *p < 0.05, **p < 0.005, ***p < 0.001, ****p < 0.0001 by one-way ANOVA with Bonferroni's correction (B) or by two-way ANOVA with Tukey's correction (A).

may thus induce an imbalance between enrichment of phylotypes that correlated positively versus negatively with tumor size, resulting in a failure to control tumor growth (Table S3).

MEKi co-administration altered the relative abundance of 21 phylotype groups (5 increased) in inulin-treated mice and of 15 phylotype groups (6 increased) in mucin-treated mice at sacrifice (Table S3). Analysis of the phylotypes in inulin+MEKi-treated mice compared with inulin-treated mice revealed four groups that negatively correlated with tumor size, based on relative abundance at sacrifice (Figure 5F). Of these, *Akkermansia*

muciniphila was robustly enriched, together with *Actinobacteria*, *Bifidobacterium longum*, *Olsenella profusa*, and *Parvibacter caecicola*. *Akkermansia muciniphila* has previously been demonstrated to possess anti-tumor properties (Routy et al., 2018). Because *Akkermansia muciniphila* was also induced in mucin+MEKi-treated mice, enrichment of this phylotype may be insufficient to control MaN-RAS tumor growth. Rather, interactions between other inulin-induced taxa may be required for *Akkermansia muciniphila* to promote the anti-tumor phenotype. The four phylotype groups that were enriched in
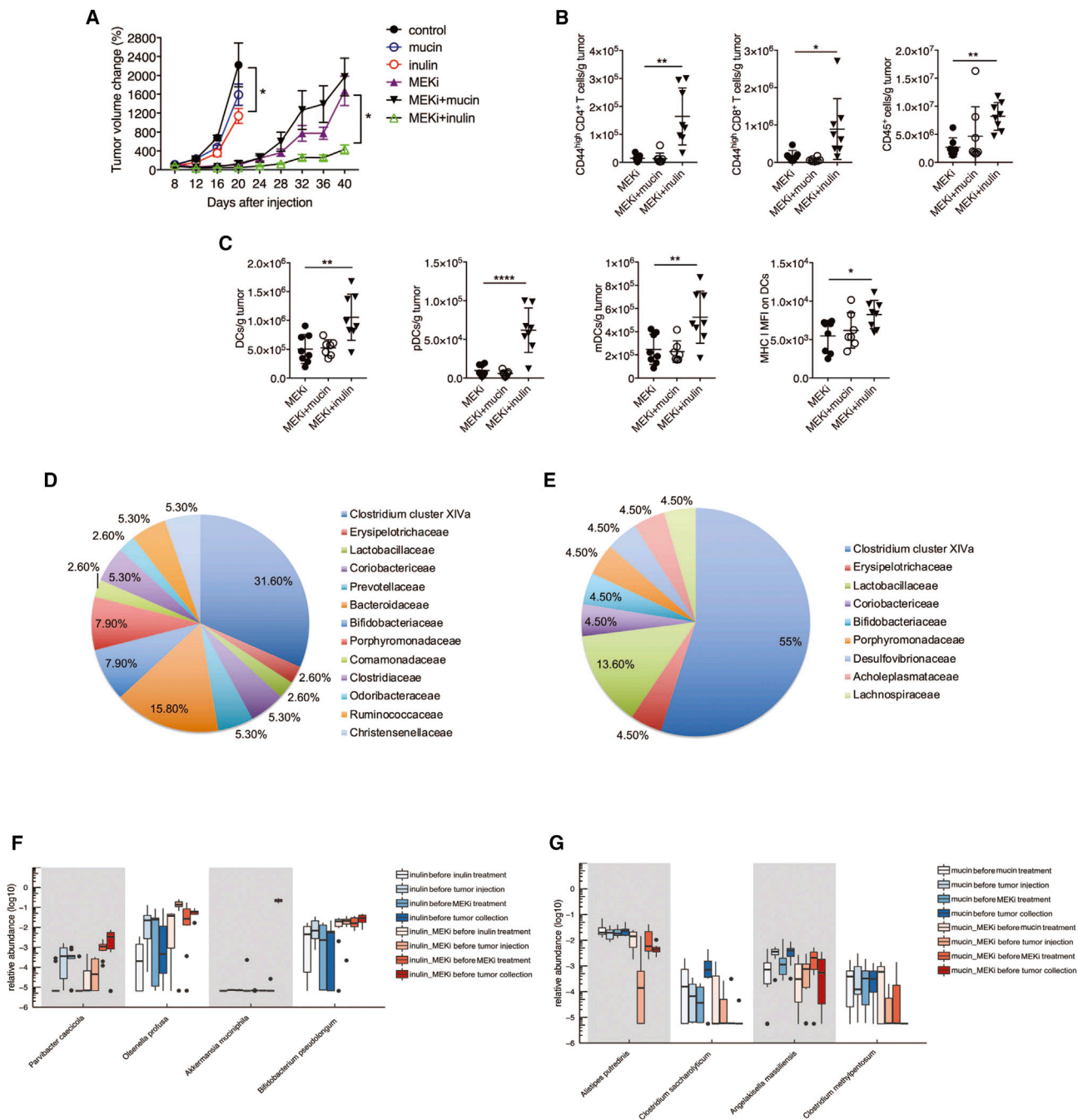
Figure 5. Inulin Supplementation Overcomes Melanoma Resistance to MEKi

(A) Growth of NRAS^Q61K mouse melanoma cells (1×10^6) (control, n = 11; mucin, n = 9; inulin, n = 9; MEKi, n = 10; MEKi+mucin, n = 8; MEKi+inulin, n = 10) that were subcutaneously transplanted in syngeneic C57BL/6 mice that received control diet, 3% mucin in drinking water, or 15% inulin-supplemented chow starting 14 days before tumor inoculation. When tumors reached a volume of 10–20 mm², mice were administered MEKi (PD325901, 10 mg/kg) once daily by gavage. Tumor volume was assessed every 4 days.

(B) Number of tumor-infiltrating effector (CD44^hi) CD4+ and CD8+ T cells and total CD45+ cells per tumor weight (in grams) in mice treated as in (A) (MEKi, n = 7; MEKi+mucin, n = 8; MEKi+inulin, n = 8).

(C) Number of tumor-infiltrating DCs and DC subsets per tumor weight (in grams) and expression of MHC class I on DCs in mice treated as in (A) (MEKi, n = 8; MEKi+mucin, n = 7; MEKi+inulin, n = 8).

(D) Pie chart of taxa enriched in inulin-treated mice and negatively correlated with MaN-RAS tumor size (n = 10).

(E) Pie chart of taxa enriched in mucin-treated mice microbiota that negatively correlate with MaN-RAS tumor size (n = 10).

(legend continued on next page)

mucin+MEKi-treated mice compared with mucin-treated mice, and that negatively correlated with tumor size, may be involved in mucin-promoted control of tumor growth (Figure 5G).

Meta-analysis of Anti-tumor Microbiota

Studies of microbiota-mediated control of tumor growth have largely focused on a single or small group of bacterial species and/or species that are over-represented in mice or humans and are positively associated with control of tumor growth. However, in the present study, we detected negative correlations between tumor size and the abundance of multiple phylogenetic clades (Figure 6), which has been difficult to reconcile with earlier studies. Some bacterial strains identified here have not previously been described to be associated with anti-tumor immunity. In addition to *Bifidobacteria*, *Bacteroides*, *Barnesiella*, and *Parabacteroides* (Daillère et al., 2016; Matson et al., 2018; Sivan et al., 2015; Tanoue et al., 2019; Vétizou et al., 2015), which have been implicated in anti-tumor responses, we identified *Olsenella*, *Prevotellamassilia*, and *Culturomica* as additional taxa whose abundance correlates with tumor size. Six members of the *Firmicutes* phylum, including taxa mapping in or near *Clostridium* cluster XIVa, were also associated with tumor growth inhibition (Figure 6).

Short-Chain Fatty Acids Are Not Sufficient to Attenuate Tumor Growth

Among the taxa enriched in gut microbiota of prebiotic-fed mice that control tumor growth are many that mapped in or near *Clostridium* cluster XIVa, which includes butyrate-producing species. We therefore next tested the effect on tumor growth of individual or combinations of the short-chain fatty acids (SCFAs) butyrate, propionate, and acetate (150 mM alone or 50 mM each in combination) administered in the drinking water starting 2 weeks before melanoma cell injection and for the duration of the experiment thereafter. None of the SCFAs, alone or in combination, reduced the tumor burden (Figure S5A), suggesting that production of SCFAs alone is insufficient to affect tumor growth.

Mucin-Induced Tumor Control Depends on Gut Microbiota

To verify the dependency of prebiotic-induced tumor control on gut microbiota, a minimal microbiota (altered Schaedler flora [ASF]) was allowed to colonize GF C3H/HeN mice for 2 weeks to induce immune maturation, and then the mice were initiated on mucin treatment for 2 weeks before injection of subcutaneously transplanted N-Ras mutant SW1 tumor cells. In these mice, mucin treatment failed to attenuate SW1 tumor growth (Figure S5B), indicating that mucin-promoted tumor growth control depends on specific gut microbiota. These observations are consistent with our previous demonstration that transfer of feces from *Rnf5*−/− mice, which harbor microbiota that can limit tumor growth, to WT GF mice elicited an effective anti-melanoma response (Li et al., 2019b).

Mucin and Inulin Treatment Leads to Activation of DCs and T Cells

To further explore the mechanism of action of mucin and inulin on the anti-tumor immune response, we treated murine bone marrow-derived DCs (BMDCs) for 24 h *in vitro* with mucin or inulin (0.05 or 0.5 mg/mL). As shown in Figure S5C, expression of the DC activation markers CD40 and CD80, as well as MHC class I and MHC class II, was increased by mucin treatment, but not inulin treatment. In contrast, *in vitro* treatment of CD8+ T cells isolated from the spleens of C57BL/6 mice revealed that whereas mucin had a limited effect on T cell activation (Figure S5D), inulin treatment increased the production of cytokines, chemokines, and the cytotoxic effector protein granzyme B (Figure S5D). These results suggest that inulin and mucin differentially affect the expression of genes involved in activation of antigen-presenting and/or effector functions of DCs and T cells. Given that mucin failed to elicit anti-tumor immunity and tumor growth inhibition in GF mice, we speculate that the effects of mucin and inulin detected *in vitro* would likely be secondary to the effects of prebiotics on the microbiota *in vivo* (Figure S5B).

Mucin and Inulin Promote Proinflammatory Gene Expression in Intestinal Epithelial Cells *In Vivo*

We next determined the effect of mucin and inulin on gene expression by intestinal epithelial cells (IECs), which have been implicated in the activation of DCs and T cells *in vivo* (Wang et al., 2003). After treatment of WT C57BL/6 with inulin or mucin for 2 weeks, IECs were isolated from the small intestine and were examined for expression of immune-related cytokines and chemokines. IECs from inulin- or mucin-treated mice exhibited enhanced expression of select genes; thus, although tumor necrosis factor alpha (TNF-α) mRNA levels were elevated in IECs from mucin-treated mice, NOD2, IL-6, and CXCL2 mRNA were increased in IECs from inulin-treated mice (Figure S5E). These findings suggest that inulin and mucin differentially enhance the transcription of key immune-activating cytokines and chemokines in IECs, providing a potential mechanism by which alterations of the gut microbiota may elicit anti-tumor immunity.

Prebiotic Therapy Does Not Augment the Efficacy of Anti-PD-1 Immune Checkpoint Therapy of Cold Melanomas

We next asked whether prebiotic treatment can enhance the efficacy of anti-PD-1 antibody, a commonly used immune checkpoint therapy. YUMM1.5, the BRAF mutant mouse melanoma cell line, is considered a cold tumor, that is, poorly responsive to immune checkpoint therapy (Haanen, 2017; Meeth et al., 2016). Administration of anti-PD-1 or the prebiotics reduced the growth of YUMM1.5 tumors in C57BL/6 mice. However, combination treatment with anti-PD-1 plus either inulin or mucin did not further attenuate tumor growth (Figures 7A and 7B), implying that anti-PD-1 and prebiotic therapy may elicit similar or overlapping changes in the immune system.

(F) Relative abundance of taxa enriched in inulin+MEKi-treated mice and negatively correlated with MaN-RAS tumor size (n = 10).

(G) Relative abundance of taxa enriched in mucin+MEKi-treated mice and negatively correlated with MaN-RAS tumor size (n = 10).

Data are representative of two independent experiments. Graphs show the mean ± SEM. *p < 0.05, **p < 0.005, ***p < 0.001, ****p < 0.0001 by one-way ANOVA with Tukey's correction (B and C) or by two-way ANOVA with Bonferroni's correction (A).
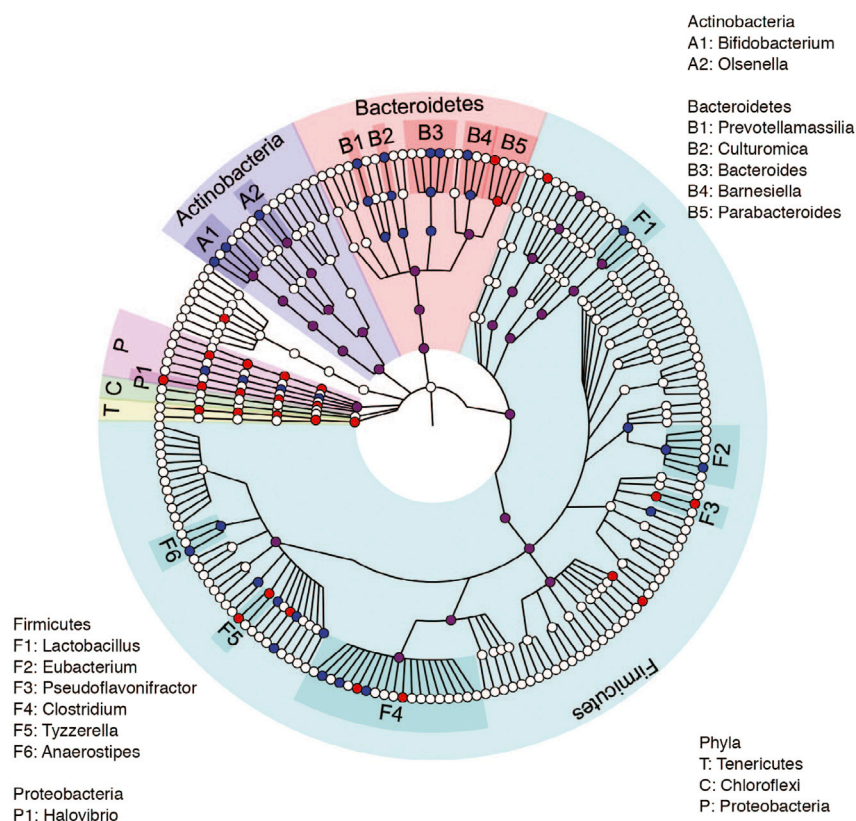
Actinobacteria
A1: Bifidobacterium
A2: Olsenella

Bacteroidetes
B1: Prevotellamassilia
B2: Culturomica
B3: Bacteroides
B4: Barnesiella
B5: Parabacteroides

Firmicutes
F1: Lactobacillus
F2: Eubacterium
F3: Pseudoflavonifractor
F4: Clostridium
F5: Tyzzerella
F6: Anaerostipes

Proteobacteria
P1: Halovibrio

Phyla
T: Tenericutes
C: Chloroflexi
P: Proteobacteria

Figure 6. A Cladogram Representation of Taxa Enriched in Fecal Microbiota of Mice Administered Mucin or Inulin

Cladogram representation of taxa enriched in fecal microbiota of mice (control, n = 12; mucin, n = 15; inulin, n = 15) administered mucin (red) or inulin (blue). Data are representative of two independent experiments.

kines and cytokines in IECs, which have known roles in the activation of DCs and T cells (Belkaid and Hand, 2014; Chistiakov et al., 2015). As a result, the growth of melanoma and/or colon cancer was attenuated, accompanied by increased infiltration of effector T cells and DCs and increased expression of immune-related genes, including chemokines and Toll-like receptor (TLRs). Notably, our studies were limited to subcutaneously implanted melanoma or colon cancer cell lines in two syngeneic mouse strains (C57BL/6 and C3H) to capture the inherent immune response. Thus, our studies did not address the complex nature of human tumors, which would be achieved using patient-derived xenografts that lack intact immune response unless carried out in humanized mouse models, and they did not examine the effect of the prebiotics studied here in genetically engineered mouse models, which could have also allowed monitoring of the effect of these prebiotics at different phases of tumor evolution and in the proper microenvironment. Heterogenous phenotypes, of both tumors and hosts, are likely to best represent the heterogeneity found in man, for which corresponding models are urgently needed.

We found that both inulin and mucin effectively limited the growth of melanoma cells, but they elicited distinct phenotypes that are likely to stem from their differential effects on gut microbiota. For example, growth of KRAS mutant MC-38 colon cancer cells was inhibited by inulin, but not by mucin. In addition, inulin combined with MEKi, but not mucin, was able to attenuate the MEKi resistance of NRAS melanoma. These data suggest that mucin and inulin elicit distinct changes in gut microbiota, which then elicit anti-tumor immunity via different mechanisms. Our results are consistent with earlier findings that inulin can inhibit tumor growth (Mauro et al., 2013; Taper and Roberfroid, 1999), although the underlying mechanism of action remained largely unexplored.

Inulin and mucin shared a common ability to promote substantial alterations in the composition of fecal microbiota, leading to increases in the relative abundance of multiple bacterial phylotypes. We observed a negative correlation between the tumor size and a subset of these phylotypes, many of which have been reported to have anti-tumor potential in independent studies. Among those are *Bifidobacterium* (Matson et al., 2018; Sivan et al., 2015), *Bacteroides* (Li et al., 2019b; Vétizou et al., 2015), *Parabacteroides* (Daillère et al., 2016; Li et al., 2019b),

Mucin and Inulin Effects on Melanoma Growth Are Context Dependent

To determine whether mucin and inulin in combination have additive or synergistic effects on melanoma growth, we employed two models. In the first, the growth of syngeneic SW1 NRAS mutant melanoma tumors that were subcutaneously transplanted in the syngeneic C3H/HeOuJ mice was attenuated by mucin treatment alone, a response that was enhanced by co-administration of mucin and inulin (Figure 7C). In contrast, growth of YUMM1.5 BRAF mutant melanoma tumors that were subcutaneously transplanted in the syngeneic C57BL/6 mice was reduced by treatment with either mucin or inulin alone, but they did not have an additive effect (Figure S6). These findings suggest that tumor genotypes and/or mouse strains affect the ability of prebiotics to attenuate tumor growth, further illustrating the complexity of the mechanisms by which gut microbiota impacts the anti-tumor phenotype.

DISCUSSION

In this study, we have demonstrated, using subcutaneously implanted tumors, that inulin and mucin induce anti-tumor immunity and concomitantly control tumor growth in syngeneic mouse models. The prebiotic effects depended on changes in the composition of gut microbiota, as illustrated by the failure of mucin to induce anti-tumor immunity in gnotobiotic mice harboring a minimal ASF community. In turn, changes in gut microbiota resulted in enhanced expression of select chemo-
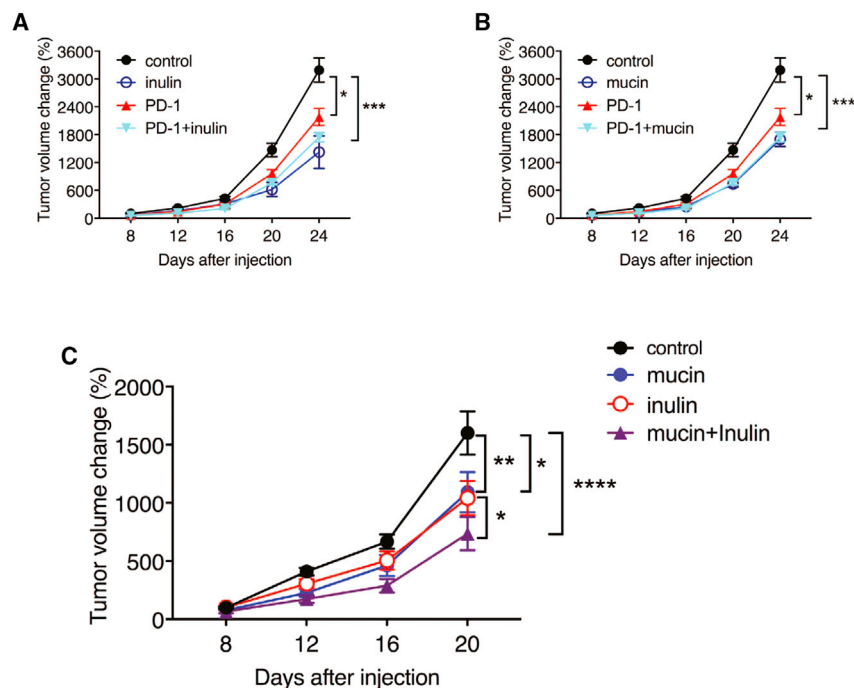
Figure 7. Combination Therapy with Prebiotics and Anti-PD-1 Modulates Tumor Growth in a Context-Dependent Manner

(A) Growth of YUMM1.5 tumors that were subcutaneously transplanted in syngeneic C57BL/6 mice that were fed control chow or chow supplemented with 15% inulin starting 14 days before tumor inoculation (control, n = 7; inulin, n = 7; PD-1, n = 10; PD-1+inulin, n = 9). Mice were injected with control IgG or anti-PD-1 blocking antibody on days 7, 10, 13, and 16 after tumor inoculation.

(B) Growth of YUMM1.5 tumors in C57BL/6 mice that received 0% or 3% mucin in drinking water starting 14 days before tumor inoculation (control, n = 7; mucin, n = 7; PD-1, n = 10; PD-1+mucin, n = 9). Mice were injected with antibodies as described in (A).

(C) Growth of SW1 mouse melanoma cells in C3H/HeOuJ mice that received a control diet, 3% mucin in drinking water, or 15% inulin-supplemented chow starting 14 days before tumor inoculation (control, n = 8; mucin, n = 8; inulin, n = 7; mucin+inulin, n = 9). Data are representative of two independent experiments. Graphs show the mean ± SEM. *p < 0.05, **p < 0.005, ***p < 0.001, ****p < 0.0001 by two-way ANOVA with Bonferroni's correction.

Akkermansia muciniphila (Routy et al., 2018), and *Barnesiella* (Daillère et al., 2016). These taxa were enriched following prebiotic feeding and MEKi treatment, pointing to their possible role in mediating tumor control. We previously observed elevated expression and post-translational modification of mucin in *Rnf5*−/− mice, which exhibit strong anti-tumor immunity, although the change in mucin expression was not accompanied by alterations in mucus thickness or intestinal leakiness (Li et al., 2019b; data not shown). Thus, modification of mucin may be one facet of crosstalk between the gut microbiota and the immune system that contributes to the anti-tumor phenotype.

Among the phylotypes induced by inulin and mucin are taxa in the butyrate-producing *Clostridium* cluster XIVa. This result is consistent with an earlier report demonstrating that over-representation of three butyrate-producing taxa was strongly associated with responsiveness to ipilimumab in human melanoma patients (Chaput et al., 2017). However, we found that butyrate, propionate, and acetate, alone or in combination, had no effect on melanoma growth, suggesting that production of other SCFAs or microbial products may mediate this microbiota-driven anti-tumor response.

Increasing attention is being paid to the effects of MEKi, which target a signaling pathway often deregulated in tumors, on immune system components (Sanlorenzo et al., 2018; Yue et al., 2018). MEKi has been shown to impede the growth of tumors in mice while concomitantly promoting the effector phenotype and longevity of tumor-infiltrating CD8+ T cells (Ebert et al., 2016). Furthermore, MEKi can promote tumor immunogenicity in preclinical models of triple-negative breast cancer, in which MEKi in combination with either anti-4-1BB or anti-OX-40 agonist antibodies resulted in superior therapeutic efficacy (Dushyanthen et al., 2017). MEKi is also capable of promoting

the maturation of DCs, as reflected by enhanced antigen uptake, processing, and cross-presentation to T cells (Vella et al., 2014). Despite effective tumor inhibition by MEKi, resistance to these inhibitors invariably occurs (Brighton et al., 2018; Fedele et al., 2018). Here, we demonstrated that co-administration of inulin reduces the resistance of melanoma to MEKi, pointing to the possible consideration of prebiotics as a means to limit therapy resistance, which remains a crucial unmet clinical need.

Several lines of evidence support the ability of microbiota to enhance the effectiveness of chemotherapy, radiotherapy, and immunotherapy (Alexander et al., 2017; Iida et al., 2013; Roy and Trinchieri, 2017). However, more recent studies have shown that antibiotic treatment or select enrichment of gut microbiota taxa can also limit the effectiveness of immune checkpoint therapy (Gopalakrishnan et al., 2018a, 2018b; Pitt et al., 2016). Thus, our finding that inulin and mucin are as effective as anti-PD-1 immune checkpoint therapy in limiting cold melanoma growth suggests that these prebiotics do not impede but possibly affect the same pathways as anti-PD-1 therapy. Combination treatment with inulin and mucin had an additive effect on the growth of NRAS mutant SW1 melanoma in C3H/HeOuJ mice, but not on the growth of YUMM1.5 BRAF mutant melanoma in C57BL/6 mice, further illustrating that the effective cooperation between prebiotics depends on both tumor and genetic background.

Collectively, the results of this study advances our understanding of tumor growth control by gut microbiota, demonstrating that taxa from multiple unrelated phylogenetic groups share the capacity to induce anti-tumor immunity. It is expected that refinement of the specific bacterial strains and metabolites that mediate these phenotypes will not only advance our understanding of the phenomenon but also facilitate the development of therapeutic modalities that could be tested across species.

STAR★METHODS

Detailed methods are provided in the online version of this paper and include the following:

- KEY RESOURCES TABLE
- LEAD CONTACT AND MATERIALS AVAILABILITY
- EXPERIMENTAL MODEL AND SUBJECT DETAILS
  - ○ Animals and tumor model
  - ○ Cell lines
  - ○ Bacterial strains and anaerobic fecal cultures
- METHOD DETAILS
  - ○ Chemically defined medium (CDM)
  - ○ Bacterial DNA extraction and 16S library preparation
  - ○ 16S sequencing data processing
  - ○ Taxa selection
  - ○ Tumor digestion
  - ○ Flow cytometry
  - ○ Mucin and inulin treatment
  - ○ RNA extraction and qRT-PCR analysis
  - ○ BMDCs
  - ○ Isolation of IECs
  - ○ Serum cytokine and chemokine detection
  - ○ *In vivo* antibody treatments
  - ○ *In vivo* OT-I T cell proliferation assay
  - ○ CD8$^+$ T cell enrichment
- QUANTIFICATION AND STATISTICAL ANALYSIS
- DATA AND CODE AVAILABILITY

SUPPLEMENTAL INFORMATION

Supplemental Information can be found online at https://doi.org/10.1016/j.celrep.2020.01.035.

AUTHOR CONTRIBUTIONS

Y.L., L.E., I.S., Y.X., R.T., Y. Feng, Y. Fu, R.S.S.M., and R.S. performed the experiments; Y.L., L.E., I.S., Y.X., R.T., L.M.B., A.R.-T., R.Z., T.L., S.N.P., and Z.A.R. analyzed the data; Z.A.R., S.N.P., T.L., R.Z., A.R.-T., L.M.B., and Y.L. designed the experiments; Z.A.R., S.N.P., L.M.B., T.L., R.Z., and Y.L. wrote the manuscript.

DECLARATION OF INTERESTS

Z.A.R. is a co-founder and serves as a scientific advisor to Pangea Therapeutics. All other authors declare no competing interests. A patent application detailing the findings disclosed in this manuscript has been filed by SBP Discovery.

REFERENCES

Adolph, T.E., Tomczak, M.F., Niederreiter, L., Ko, H.J., Böck, J., Martinez-Naves, E., Glickman, J.N., Tschurtschenthaler, M., Hartwig, J., Hosomi, S., et al. (2013). Paneth cells as a site of origin for intestinal inflammation. Nature 503, 272–276.

Alexander, J.L., Wilson, I.D., Teare, J., Marchesi, J.R., Nicholson, J.K., and Kinross, J.M. (2017). Gut microbiota modulation of chemotherapy efficacy and toxicity. Nat. Rev. Gastroenterol. Hepatol. 14, 356–365.

Apte, R.N., Dotan, S., Elkabets, M., White, M.R., Reich, E., Carmi, Y., Song, X., Dvozkin, T., Krelin, Y., and Voronov, E. (2006). The involvement of IL-1 in tumorigenesis, tumor invasiveness, metastasis and tumor-host interactions. Cancer Metastasis Rev. 25, 387–408.

Arthur, J.C., Perez-Chanona, E., Mühlbauer, M., Tomkovich, S., Uronis, J.M., Fan, T.J., Campbell, B.J., Abujamel, T., Dogan, B., Rogers, A.B., et al. (2012). Intestinal inflammation targets cancer-inducing activity of the microbiota. Science 338, 120–123.

Bäckhed, F., Ley, R.E., Sonnenburg, J.L., Peterson, D.A., and Gordon, J.I. (2005). Host-bacterial mutualism in the human intestine. Science 307, 1915–1920.

Belkaid, Y., and Hand, T.W. (2014). Role of the microbiota in immunity and inflammation. Cell 157, 121–141.

Bellone, M., Cantarella, D., Castiglioni, P., Crosti, M.C., Ronchetti, A., Moro, M., Garancini, M.P., Casorati, G., and Dellabona, P. (2000). Relevance of the tumor antigen in the validation of three vaccination strategies for melanoma. J. Immunol. 165, 2651–2656.

Bhoumik, A., Huang, T.G., Ivanov, V., Gangi, L., Qiao, R.F., Woo, S.L., Chen, S.H., and Ronai, Z. (2002). An ATF2-derived peptide sensitizes melanomas to apoptosis and inhibits their growth and metastasis. J. Clin. Invest. 110, 643–650.

Bonnet, M., Buc, E., Sauvanet, P., Darcha, C., Dubois, D., Pereira, B., Déchelotte, P., Bonnet, R., Pezet, D., and Darfeuille-Michaud, A. (2014). Colonization of the human gut by *E. coli* and colorectal cancer risk. Clin. Cancer Res. 20, 859–867.

Brighton, H.E., Angus, S.P., Bo, T., Roques, J., Tagliatela, A.C., Darr, D.B., Karagoz, K., Sciaky, N., Gatza, M.L., Sharpless, N.E., et al. (2018). New Mechanisms of Resistance to MEK Inhibitors in Melanoma Revealed by Intravital Imaging. Cancer Res. 78, 542–557.

Chaput, N., Lepage, P., Coutzac, C., Soularue, E., Le Roux, K., Monot, C., Boselli, L., Routier, E., Cassard, L., Collins, M., et al. (2017). Baseline gut microbiota predicts clinical response and colitis in metastatic melanoma patients treated with ipilimumab. Ann. Oncol. 28, 1368–1379.

Chistiakov, D.A., Bobryshev, Y.V., Kozarov, E., Sobenin, I.A., and Orekhov, A.N. (2015). Intestinal mucosal tolerance and impact of gut microbiota to mucosal tolerance. Front. Microbiol. 5, 781.

Colli, L.M., Machiela, M.J., Zhang, H., Myers, T.A., Jessop, L., Delattre, O., Yu, K., and Chanock, S.J. (2017). Landscape of Combination Immunotherapy and Targeted Therapy to Improve Cancer Management. Cancer Res. 77, 3666–3671.

Daillère, R., Vétizou, M., Waldschmitt, N., Yamazaki, T., Isnard, C., Poirier-Colame, V., Duong, C.P.M., Flament, C., Lepage, P., Roberti, M.P., et al. (2016). *Enterococcus hirae* and *Barnesiella intestinihominis* Facilitate Cyclophosphamide-Induced Therapeutic Immunomodulatory Effects. Immunity 45, 931–943.

Dapito, D.H., Mencin, A., Gwak, G.Y., Pradere, J.P., Jang, M.K., Mederacke, I., Caviglia, J.M., Khiabanian, H., Adeyemi, A., Bataller, R., et al. (2012). Promotion of hepatocellular carcinoma by the intestinal microbiota and TLR4. Cancer Cell 21, 504–516.

Dushyanthen, S., Teo, Z.L., Caramia, F., Savas, P., Mintoff, C.P., Virassamy, B., Henderson, M.A., Luen, S.J., Mansour, M., Kershaw, M.H., et al. (2017). Agonist immunotherapy restores T cell function following MEK inhibition improving efficacy in breast cancer. Nat. Commun. 8, 606.

Ebert, P.J.R., Cheung, J., Yang, Y., McNamara, E., Hong, R., Moskalenko, M., Gould, S.E., Maecker, H., Irving, B.A., Kim, J.M., et al. (2016). MAP Kinase

Inhibition Promotes T Cell and Anti-tumor Activity in Combination with PD-L1 Checkpoint Blockade. Immunity 44, 609–621.

Eggermont, A.M.M., Crittenden, M., and Wargo, J. (2018). Combination Immunotherapy Development in Melanoma. Am. Soc. Clin. Oncol. Educ. Book 38, 197–207.

Everard, A., Belzer, C., Geurts, L., Ouwerkerk, J.P., Druart, C., Bindels, L.B., Guiot, Y., Derrien, M., Muccioli, G.G., Delzenne, N.M., et al. (2013). Crosstalk between Akkermansia muciniphila and intestinal epithelium controls diet-induced obesity. Proc. Natl. Acad. Sci. USA 110, 9066–9071.

Fedele, C., Ran, H., Diskin, B., Wei, W., Jen, J., Geer, M.J., Araki, K., Ozerdem, U., Simeone, D.M., Miller, G., et al. (2018). SHP2 Inhibition Prevents Adaptive Resistance to MEK Inhibitors in Multiple Cancer Models. Cancer Discov. 8, 1237–1249.

Fehlbaum, S., Prudence, K., Kieboom, J., Heerikhuisen, M., van den Broek, T., Schuren, F.H.J., Steinert, R.E., and Raederstorff, D. (2018). In Vitro Fermentation of Selected Prebiotics and Their Effects on the Composition and Activity of the Adult Gut Microbiota. Int. J. Mol. Sci. 19, E3097.

Gomes-Neto, J.C., Mantz, S., Held, K., Sinha, R., Segura Munoz, R.R., Schmaltz, R., Benson, A.K., Walter, J., and Ramer-Tait, A.E. (2017). A realtime PCR assay for accurate quantification of the individual members of the Altered Schaedler Flora microbiota in gnotobiotic mice. J. Microbiol. Methods 135, 52–62.

Gopalakrishnan, V., Helmink, B.A., Spencer, C.N., Reuben, A., and Wargo, J.A. (2018a). The Influence of the Gut Microbiome on Cancer, Immunity, and Cancer Immunotherapy. Cancer Cell 33, 570–580.

Gopalakrishnan, V., Spencer, C.N., Nezi, L., Reuben, A., Andrews, M.C., Karpinets, T.V., Prieto, P.A., Vicente, D., Hoffman, K., Wei, S.C., et al. (2018b). Gut microbiome modulates response to anti-PD-1 immunotherapy in melanoma patients. Science 359, 97–103.

Haanen, J.B.A.G. (2017). Converting Cold into Hot Tumors by Combining Immunotherapies. Cell 170, 1055–1056.

Haapanen, M.L., Kalland, M., Heliövaara, A., Hukki, J., and Ranta, R. (1997). Velopharyngeal function in cleft patients undergoing maxillary advancement. Folia Phoniatr. Logop. 49, 42–47.

Hampton, T.A., Conry, R.M., Khazaeli, M.B., Shaw, D.R., Curiel, D.T., LoBuglio, A.F., and Strong, T.V. (2000). SEREX analysis for tumor antigen identification in a mouse model of adenocarcinoma. Cancer Gene Ther. 7, 446–455.

Humphries, A., and Daud, A. (2018). The gut microbiota and immune checkpoint inhibitors. Hum. Vaccin. Immunother. 14, 2178–2182.

Iida, N., Dzutsev, A., Stewart, C.A., Smith, L., Bouladoux, N., Weingarten, R.A., Molina, D.A., Salcedo, R., Back, T., Cramer, S., et al. (2013). Commensal bacteria control cancer response to therapy by modulating the tumor microenvironment. Science 342, 967–970.

Johnson, D.B., and Puzanov, I. (2015). Treatment of NRAS-mutant melanoma. Curr. Treat. Options Oncol. 16, 15.

Laukens, D., Brinkman, B.M., Raes, J., De Vos, M., and Vandenabeele, P. (2016). Heterogeneity of the gut microbiome in mice: guidelines for optimizing experimental design. FEMS Microbiol. Rev. 40, 117–132.

Ley, R.E., Lozupone, C.A., Hamady, M., Knight, R., and Gordon, J.I. (2008). Worlds within worlds: evolution of the vertebrate gut microbiota. Nat. Rev. Microbiol. 6, 776–788.

Li, X., Leonardi, I., Semon, A., Doron, I., Gao, I.H., Putzel, G.G., Kim, Y., Kabata, H., Artis, D., Fiers, W.D., et al. (2018). Response to Fungal Dysbiosis by Gut-Resident CX3CR1(+) Mononuclear Phagocytes Aggravates Allergic Airway Disease. Cell Host Microbe 24, 847–856.

Li, K., Zhang, L., Xue, J., Yang, X., Dong, X., Sha, L., Lei, H., Zhang, X., Zhu, L., Wang, Z., et al. (2019a). Dietary inulin alleviates diverse stages of type 2 diabetes mellitus via anti-inflammation and modulating gut microbiota in db/db mice. Food Funct. 10, 1915–1927.

Li, Y., Tinoco, R., Elmén, L., Segota, I., Xian, Y., Fujita, Y., Sahu, A., Zarecki, R., Marie, K., Feng, Y., et al. (2019b). Gut microbiota dependent anti-tumor immunity restricts melanoma growth in Rnf5−/− mice. Nat. Commun. 10, 1492.

Martz, C.A., Ottina, K.A., Singleton, K.R., Jasper, J.S., Wardell, S.E., Peraza-Penton, A., Anderson, G.R., Winter, P.S., Wang, T., Alley, H.M., et al. (2014). Systematic identification of signaling pathways with potential to confer anticancer drug resistance. Sci. Signal. 7, ra121.

Matson, V., Fessler, J., Bao, R., Chongsuwat, T., Zha, Y., Alegre, M.L., Luke, J.J., and Gajewski, T.F. (2018). The commensal microbiome is associated with anti-PD-1 efficacy in metastatic melanoma patients. Science 359, 104–108.

Mauro, M.O., Monreal, M.T., Silva, M.T., Pesarini, J.R., Mantovani, M.S., Ribeiro, L.R., Dichi, J.B., Carreira, C.M., and Oliveira, R.J. (2013). Evaluation of the antimutagenic and anticarcinogenic effects of inulin in vivo. Genet. Mol. Res. 12, 2281–2293.

Meeth, K., Wang, J.X., Micevic, G., Damsky, W., and Bosenberg, M.W. (2016). The YUMM lines: a series of congenic mouse melanoma cell lines with defined genetic alterations. Pigment Cell Melanoma Res. 29, 590–597.

Petit, V., Raymond, J., Alberti, C., Pouteaux, M., Gallagher, S.J., Nguyen, M.Q., Aplin, A.E., Delmas, V., and Larue, L. (2019). C57BL/6 congenic mouse NRAS^{Q61K} melanoma cell lines are highly sensitive to the combination of Mek and Akt inhibitors in vitro and in vivo. Pigment Cell Melanoma Res. 32, 829–841.

Pitt, J.M., Vétizou, M., Waldschmitt, N., Kroemer, G., Chamaillard, M., Boneca, I.G., and Zitvogel, L. (2016). Fine-Tuning Cancer Immunotherapy: Optimizing the Gut Microbiome. Cancer Res. 76, 4602–4607.

Ribas, A., Lawrence, D., Atkinson, V., Agarwal, S., Miller, W.H., Jr., Carlino, M.S., Fisher, R., Long, G.V., Hodi, F.S., Tsoi, J., et al. (2019). Combined BRAF and MEK inhibition with PD-1 blockade immunotherapy in BRAF-mutant melanoma. Nat. Med. 25, 936–940.

Routy, B., Le Chatelier, E., Derosa, L., Duong, C.P.M., Alou, M.T., Daillère, R., Fluckiger, A., Messaoudene, M., Rauber, C., Roberti, M.P., et al. (2018). Gut microbiome influences efficacy of PD-1-based immunotherapy against epithelial tumors. Science 359, 91–97.

Roy, S., and Trinchieri, G. (2017). Microbiota: a key orchestrator of cancer therapy. Nat. Rev. Cancer 17, 271–285.

Rutkowski, M.R., Stephen, T.L., Svoronos, N., Allegrezza, M.J., Tesone, A.J., Perales-Puchalt, A., Brencicova, E., Escovar-Fadul, X., Nguyen, J.M., Cadungog, M.G., et al. (2015). Microbially driven TLR5-dependent signaling governs distal malignant progression through tumor-promoting inflammation. Cancer Cell 27, 27–40.

Sanlorenzo, M., Vujic, I., Floris, A., Novelli, M., Gammaitoni, L., Giraudo, L., Macagno, M., Leuci, V., Rotolo, R., Donini, C., et al. (2018). BRAF and MEK Inhibitors Increase PD-1-Positive Melanoma Cells Leading to a Potential Lymphocyte-Independent Synergism with Anti-PD-1 Antibody. Clin. Cancer Res. 24, 3377–3385.

Singh, A., Zapata, R.C., Pezeshki, A., Reidelberger, R.D., and Chelikani, P.K. (2018). Inulin fiber dose-dependently modulates energy balance, glucose tolerance, gut microbiota, hormones and diet preference in high-fat-fed male rats. J. Nutr. Biochem. 59, 142–152.

Sivan, A., Corrales, L., Hubert, N., Williams, J.B., Aquino-Michaels, K., Earley, Z.M., Benyamin, F.W., Lei, Y.M., Jabri, B., Alegre, M.L., et al. (2015). Commensal Bifidobacterium promotes antitumor immunity and facilitates anti-PD-L1 efficacy. Science 350, 1084–1089.

Sommer, F., and Bäckhed, F. (2013). The gut microbiota—masters of host development and physiology. Nat. Rev. Microbiol. 11, 227–238.

Tanoue, T., Morita, S., Plichta, D.R., Skelly, A.N., Suda, W., Sugiura, Y., Narushima, S., Vlamakis, H., Motoo, I., Sugita, K., et al. (2019). A defined commensal consortium elicits CD8 T cells and anti-cancer immunity. Nature 565, 600–605.

Taper, H.S., and Roberfroid, M. (1999). Influence of inulin and oligofructose on breast cancer and tumor growth. J. Nutr. 129 (Suppl 7), 1488S–1491S.

Vella, L.J., Pasam, A., Dimopoulos, N., Andrews, M., Knights, A., Puaux, A.L., Louahed, J., Chen, W., Woods, K., and Cebon, J.S. (2014). MEK inhibition, alone or in combination with BRAF inhibition, affects multiple functions of

isolated normal human lymphocytes and dendritic cells. Cancer Immunol. Res. 2, 351–360.

Vétizou, M., Pitt, J.M., Daillère, R., Lepage, P., Waldschmitt, N., Flament, C., Rusakiewicz, S., Routy, B., Roberti, M.P., Duong, C.P., et al. (2015). Anticancer immunotherapy by CTLA-4 blockade relies on the gut microbiota. Science 350, 1079–1084.

Wang, L., Walia, B., Evans, J., Gewirtz, A.T., Merlin, D., and Sitaraman, S.V. (2003). IL-6 induces NF-kappa B activation in the intestinal epithelia. J. Immunol. 171, 3194–3201.

Wang, L., Yi, T., Kortylewski, M., Pardoll, D.M., Zeng, D., and Yu, H. (2009). IL-17 can promote tumor growth through an IL-6-Stat3 signaling pathway. J. Exp. Med. 206, 1457–1464.

York, A. (2018). Microbiome: Gut microbiota sways response to cancer immunotherapy. Nat. Rev. Microbiol. 16, 121.

Yue, P., Harper, T., Bacot, S.M., Chowdhury, M., Lee, S., Akue, A., Kukuruga, M.A., Wang, T., and Feldman, G.M. (2018). BRAF and MEK inhibitors differentially affect nivolumab-induced T cell activation by modulating the TCR and AKT signaling pathways. OncoImmunology 8, e1512456.

STAR★METHODS

KEY RESOURCES TABLE

REAGENT or RESOURCE	SOURCE	IDENTIFIER
Antibodies		
Purified anti-mouse CD16/32	BioLegend	Cat#101302; clone 93; RRID: AB_312800
PerCP anti-mouse CD45.2	BioLegend	Cat# 109826; clone 104; RRID: AB_893349
Pacific Blue anti-mouse CD8a	BioLegend	Cat# 100725; clone 53–6.7; RRID: AB_493425
Brilliant Violet 605 anti-mouse CD4	BioLegend	Cat# 100451; clone GK1.5; RRID:AB_2564591
FITC anti-mouse CD25	BioLegend	Cat# 101908; clone 3C7; RRID: AB_961210
APC/Cy7 anti-mouse/human CD44	BioLegend	Cat# 103028; clone IM7; RRID: AB_830785
PE/Cy7 anti-mouse TNF-α	BioLegend	Cat# 506324; clone MP6-XT22; RRID: AB_2204356
APC anti-mouse IFN-γ	BioLegend	Cat# 505810; clone XMG1.2; RRID: AB_315403
APC anti-mouse CD11c	BioLegend	Cat# 117310; clone N418; RRID: AB_313778
APC anti-mouse CD103	BioLegend	Cat# 121414; clone 2E7; RRID: AB_1227503
FITC anti-mouse H-2Kb	BioLegend	Cat# 116506; clone AF6–88.5; RRID: AB_313733
Pacific Blue anti-mouse I-A/I-E	BioLegend	Cat# 107620; clone M5/114.15.2; RRID: AB_493527
FITC anti-mouse CD45.1	BioLegend	Cat# 110706; clone A20; RRID: AB_313495
APC/Cy7 anti-mouse/human CD11b	BioLegend	Cat# 101225; clone M1/70; RRID: AB_830641
PE anti-mouse CD317 (BST2, PDCA-1)	BioLegend	Cat#127104; clone129C1; RRID: AB_1953283
FITC anti-mouse/human IL-2	eBioscience	Cat# 11-7021-41; clone JES6-5H4; RRID: AB_10734043
FITC anti-mouse/human MHC Class I	eBioscience	Cat# 11-5958-82; clone AF6-88.5.5.3; RRID: AB_11149502
PE/Cy7 anti-mouse/human CD45R/B220	BioLegend	Cat# 103222; clone RA3-6B2; RRID: AB_313005
GoInVivo Purified anti-mouse CD279 (PD-1)	BioLegend	Cat# 114112; clone RMP1-14; RRID: AB_2566090
GoInVivo Purified Rat IgG2a, κ Isotype Ctrl	BioLegend	Cat#400560; clone RTK2758
InVivoMAb anti-mouse Thy1.2 (CD90.2)	BioXCell	Cat# BE0066; clone 30H12; AB_1107682
Bacterial and Virus Strains		
ASF	(Li et al., 2018)	N/A
Chemicals, Peptides, and Recombinant Proteins		
GM-CSF	BioLegend	Cat# 576306
CFSE (carboxyfluorescein succinimidyl easter)	Thermo Fisher Scientific	Cat# C34554
Collagenase D	Roche	Cat #11088882001
DNase	Sigma	Cat #DN25-1G
Brefeldin A	Sigma	Cat# B7651-5MG
Phorbol 12-myristate 13-acetate	Sigma	Cat# P8139-1MG
Ionomycin calcium salt	Sigma	Cat# 3909-1ML
Mucin	Lee Biosolutions	Cat# 435-10
Dulbecco's modified Eagle's medium (DMEM)	Corning	Cat# 10-013-CV
Fetal bovine serum (FBS)	Gemini Bioproducts	Cat#900-208
Penicillin (100 units/mL) and Streptomycin (100 ug/mL)	Corning	Cat#30-002-CI
Trypsin-EDTA (0.25%), phenol red	Fisher Scientific	Cat#25200056
DPBS without Mg2+ and Ca^{2+}	Corning	Cat#21-031-CV
HBSS without Mg2+ and Ca^{2+}	Corning	Cat#21021152
RBC lysis buffer	Sigma	Cat#R7757
HEPES Buffer	Corning	Cat#25-060-CI
2-mercaptoethanol	Sigma	Cat#133051

(Continued on next page)

Continued

REAGENT or RESOURCE	SOURCE	IDENTIFIER
Critical Commercial Assays		
RNeasy Plus Mini Kit	QIAGEN	Cat#74134
LEGENDplex mouse inflammation panel	BioLegend	Cat#740446
LEGENDplex mouse proinflammatory chemokine panel	BioLegend	Cat#740451
RNeasy Fibrous Tissue Mini kit	QIAGEN	Cat#74704
High Capacity Reverse Transcriptase kits	Invitrogen	Cat#4368814
SYBR Green RT-PCR kits	Invitrogen	Cat#4385610
BD Cytofix/Cytoperm	BD Biosciences	Cat#554714
QIAquick 96-PCR Cleanup kit	QIAGEN	Cat#28181
QIAamp Fast DNA Stool Mini Kit	QIAGEN	Cat#51604
Deposited Data		
Bacterial 16 s sequence	This paper	The approach used to map microbiota taxa is detailed at: http://github.com/taolonglab/himap; BioRxiv 565572. The microbiome sequence data have been deposited in the NCI BioProject: PRJNA593851 https://www.ncbi.nlm.nih.gov/bioproject/PRJNA593851
Raw data	This paper	The raw data were deposited to Mendeley https://data.mendeley.com/datasets/zrjr39f7mb/draft?a=28ed04b4-6d90-4eec-be59-c42e05589ade.
Experimental Models: Cell Lines		
Mouse: YUMM1.5	Gift from Marcus Bosenberg (Meeth et al., 2016)	N/A
Mouse: MC-38	Gift from Michael Karin (Li et al., 2019b)	N/A
Mouse: MaN-RASQ61K	Gift from Lionel Larue (Petit et al., 2019)	N/A
Mouse: SW1	Gift from Margaret Kripke (Bhoumik et al., 2002)	N/A
Mouse: B16-OVA	Gift from Linda Bradley (Li et al., 2019b)	N/A
Experimental Models: Organisms/Strains		
Mouse: C57BL/6	Sanford Burnham Prebys Medical Discovery Institute	N/A
Mouse: CD45.1 (B6.SJLB6.SJL-Ptprca Pepcb/BoyJ)	The Jackson Laboratory	Stock No: 002014
Mouse: C3H/HeOuJ	The Jackson Laboratory	Stock No: 000635
Mouse: EX-germ-free ASF-bearing C3H/HeN	University of Nebraska-Lincoln (UNL)	N/A
Oligonucleotides		
qPCR primer sequences, See Table S4	This paper	N/A
V3-V4 Forward primer: TCGTCGGCAGCGTCAGAT GTGTATAAGAGACAGCCTACGGGNGGCWGCAG	This paper	N/A
V3-V4 Reverse primer: GTCTCGTGGGCTCGGAG ATGTGTATAAGAGACAG GACTACHVGGGTATCT AATCC	This paper	N/A
Software and Algorithms		
GraphPad Prism 6 and 7	Graphpad Software	N/A
FlowJo v10.1 and v9.9	Treestar	N/A
FACSDiva Software	BD	N/A
Algorithms HiMAP	This paper	N/A
LEGENDplexTM	BioLegend	N/A

REAGENT or RESOURCE	SOURCE	IDENTIFIER
Other		
100 um cell strainer	Thermo Fisher	Cat# 22363549
Purified Diet, AIN-93M,	ENVIGO	TD. 94048,
Modified AIN-93M, Diet w 15% inulin,	ENVIGO	TD. 160256
Chow diet *ad libitum* (Purina Foods)	LabDiet	Form: 5K67

LEAD CONTACT AND MATERIALS AVAILABILITY

Further information and requests for reagents should be directed to and will be fulfilled by the Lead contact, Ze'ev Ronai, at zeev@ronailab.net. All reagents generated in this study are available from the Lead Contact with a completed Materials Transfer Agreement.

EXPERIMENTAL MODEL AND SUBJECT DETAILS

Animals and tumor model

All experimental animal procedures were approved by the Institutional Animal Care and Use Committee of Sanford Burnham Prebys Medical Discovery Institute (SBP: approval #13-130, 16-028, and 17-001) and complied with all relevant ethical regulations for animal testing and research. C57BL/6 mice were obtained from SBP. OT-I mice were obtained from SBP and crossed to CD45.1[+] B6.SJLB6.SJL-*Ptprc*[a] *Pepc*[b]/BoyJ mice (Jackson Laboratories). C3H/HeOuJ mice were purchased from Jackson Laboratories. Male 6–8-week-old mice were used for all experiments. GF ASF-bearing C3H/HeN mice were bred and maintained at the University of Nebraska-Lincoln (UNL) Gnotobiotic Mouse Facility under gnotobiotic conditions in flexible film isolators. Experiments involving GF and gnotobiotic mice were approved by the Institutional Animal Care and Use Committee at UNL (protocol #1534). All mice were fed an autoclaved chow diet *ad libitum* (LabDiet 5K67, Purina Foods). GF status was routinely checked as previously described (Gomes-Neto et al., 2017). Briefly, fresh feces were collected and analyzed by bacterial 16S rRNA gene-specific PCR (30 cycles, universal bacteria primers 8F and 1391R) in combination with aerobic and anaerobic culture of feces in Brain Heart Infusion, Wilkins–Chalgren, and Yeast Mold broths, and on Tryptic Soy Agar plates (all media from Difco Becton Dickinson) at 37°C for 7 days. ASF colonization status was verified by qPCR analysis of fecal samples as previously described (Li et al., 2019b). Briefly, genomic DNA was extracted from fecal samples and ASF bacteria were quantified by qPCR with species-specific primers.

For tumor growth experiments, mice were injected subcutaneously (s.c.) with 1×10^6 tumor cells. Tumor size was measured twice a week for calculation of tumor volume. Tumors were weighed at the time of excision. Mouse selection for experiments was not formally randomized or blinded.

Cell lines

Braf[V600E/+]*;Pten*^{−/−}*;Cdkn2a*^{−/−} mouse melanoma cell line YUMM1.5 (Meeth et al., 2016), MC-38 cells ((Hampton et al., 2000); provided by M Karin, UCSD), MaN-RAS[Q61K] mouse melanoma cells ((Petit et al., 2019); Provided by Lionel Larue, CNRS) SW1 mouse melanoma cells ((Bhoumik et al., 2002); provided by M Kripke, MDACC) B16-OVA ((Bellone et al., 2000); Provided by L Bradley SBP). Cell lines were maintained in Dulbecco's modified Eagle's medium supplemented with 10% fetal bovine serum (FBS) and antibiotics. All cell lines were free of mycoplasma and were authenticated by SBP genomic core service.

Bacterial strains and anaerobic fecal cultures

ASF (Altered Schaedler Flora) consisted of the following eight isolates: ASF 356, *Clostridium* sp.; ASF 360, *Lactobacillus intestinalis*; ASF 361, *Lactobacillus murinus*; ASF 457, *Mucispirillum schaedleri*; ASF 492, *Eubacterium plexicaudatum*; ASF 500, *Pseudoflavonifractor* sp.; ASF 502, *Clostridium* sp.; and ASF 519, *Parabacteroides goldsteinii*. Stool collected from 12 healthy vegetarian volunteers or WT mice (approximately 10^6 cells) were inoculated into chemically defined medium (CDM) alone or supplemented with 1% inulin or 1% porcine gastric mucin in Hungate tubes. Anaerobic cultures (9% H_2, 81% N_2) were grown statically for 3–4 days at 3°C to approximate saturation.

METHOD DETAILS

Chemically defined medium (CDM)

CDM contained 50 mM HEPES, 2.2 mM KH2PO4, 10 mM Na2HPO4, 60 mM NaHCO3; 4 mM of each amino acid except leucine (15 mM); 10 mL ATCC Trace Mineral Supplement; nucleoside bases (100 mg/L) inosine, xanthine, adenine, guanine, cytosine, thymidine, and uracil (400 mg/L); choline (100 mg/L), ascorbic acid (500 mg/L), lipoic acid (2 mg/L), hemin (1.2 mg/L), and myo-inositol (400 mg/L). Resazurin (1 mg/L) was added to visually monitor dissolved oxygen. The pH was adjusted to 7.4.

Bacterial DNA extraction and 16S library preparation

Gut microbiota in the mouse reach a stable homeostatic state at about 8 weeks of age (Laukens et al., 2016). Fecal pellets from mice ≥ 8 weeks of age were frozen on dry ice and stored at −80°C. Bacterial DNA was extracted using a QIAmp Fast DNA Stool Mini Kit (QIAGEN) with an additional 5-min bead-beating step using a Mini-Beadbeater-16 (Biospec Products, OK, USA). Library preparation for the Illumina MiSeq platform was performed by amplification of the V3-V4 region of the bacterial 16S ribosomal DNA gene using forward primer: 5′-TCGTCGGCAGCGTCAGATGTGTATAAGAGACAGCCTACGGGNGGCWGCAG and reverse primer: 5′-GTCTCG TGGGCTCGGAGATGTGTATAAGAGACAG GACTACHVGGGTATCTAATCC. Adaptor and barcode sequences for dual indices were used as described by Illumina. PCR cleanup steps were performed using a QIAquick 96-PCR Cleanup Kit (QIAGEN, Germany), and library quantification was performed using a KAPA Library Quantification Kit for Illumina platforms (KAPA Biosystems, MA, USA). An Experion Automated Gel Electrophoresis System (Bio-Rad, CA, USA) was used to measure the DNA concentration and purity in the pooled libraries. The 16S libraries were sequenced at Novagene (Beijing, China) and at the SBP sequencing core.

16S sequencing data processing

The original FASTQ files from Illumina 250 base-pair paired-end sequencing were processed using a 16S amplicon sequencing pipeline HiMap (http://github.com/taolonglab/himap; BioRxiv 565572). The output of HiMap is Operational Strain Unit (OSU) which contains one or more bacterial strains that best match the 16S sequence and cannot be further distinguished. The percentage similarity between the 16S sequence and the aligned region of 16S rRNA genes of the strains in the OSU is indicated. OSUs mapped to the same strains are grouped together (adding read counts) if percentage similarities are within 3%. Read counts are converted into relative abundance as described in HiMap. Log10-transformed relative abundances were used for comparisons between samples under different experimental conditions. The raw 16S sequencing data is available as BioProject PRJNA593851 online at: https://www. ncbi.nlm.nih.gov/bioproject/PRJNA593851.

Taxa selection

Taxa that distinguished microbiota of inulin- or mucin-treated mice from control mice were selected into three sets as follows. (1) Taxa induced by inulin or mucin were selected by performing a paired one-tail Wilcoxon rank-sum test on the log10-transformed relative abundances of all OSU groups in mice treated with prebiotics at time point B (after the start of prebiotic treatment and before tumor injection) compared with time point A (before prebiotic treatment) with abundance at time point B greater than time point A. Taxa with p values less than 0.05 were selected as set 1. (2) A similar selection to (1) was made for data from the control mice. Taxa with p values less than 0.2 were selected as set 2. This set contains taxa that were induced in the control group from time point A to time point B. (3) The third set of OSU groups were selected by calculating Spearman's correlations between each of the OSU groups and tumor size at time point B, and selecting groups with p values less than 0.1. The final set of inulin- or mucin-induced taxa was selected as the difference between set 1 and set 2 intersected with set 3. These are the taxa induced in inulin- or mucin-treated mice, but not in control mice, and had relative abundances before tumor injection that negatively correlated with tumor size at tumor collection. For analysis of mice treated with MEKi in combination with prebiotics, OSU groups in the fecal samples of mice treated with prebiotics alone or in combination with MEKi were compared at time point D (final time point before tumor collection) with unpaired two-sided Wilcoxon rank-sum test. OSU groups with p values less than 0.05 were selected for calculating Spearman's correlations with tumor size at time point D. The OSU groups with correlation p values less than 0.1 were selected as the differential taxa that were negatively correlated with tumor size.

Tumor digestion

Tumors were excised, minced, and digested with 1 mg/mL collagenase D (Roche) and 100 μg/mL DNase I (Sigma) at 37°C for 1 h. Digests were then passed through a 70-μm cell strainer to generate a single-cell suspension. The cells were washed twice with PBS containing 2 mM EDTA and then stained for flow cytometry.

Flow cytometry

Tumor-derived single-cell suspensions were washed twice with FACS staining buffer, fixed for 15 min with 1% formaldehyde in PBS, washed twice, and resuspended in FACS staining buffer. For intracellular cytokine staining, cells were resuspended in complete RPMI-1640 (containing 10 mM HEPES, 1% non-essential amino acids and L-glutamine, 1 mM sodium pyruvate, 10% heat-inactivated FBS, and antibiotics) supplemented with 50 U/mL IL-2 (NCI) and 1 mg/mL brefeldin A (BFA, Sigma), and then incubated with phorbol myristate acetate (10 ng/mL) and ionomycin (0.5 μg/mL) at 37°C. The cells were fixed and permeabilized using a Cytofix/Cytoperm Kit (BD Biosciences) before staining. Antibodies to the following proteins were used: CD45.2 (104), CD8α (53-6.7), CD4 (GK1.5), CD44 (IM7), TNF-α (MP6-XT22), IFN-γ (XMG1.2), CD11c (N418), CD11b (M1/70), MHC class II (M5/114.15.2), PDCA (129c1), and B220 (RA3-6B2) (all from BioLegend), IL-2 (JES6-5H4) and MHC class I (AF6-88.5.5.3) (both from eBioscience). All data were collected on an LSRFortessa (BD Biosciences) and analyzed using FlowJo Software (Tree Star).

Mucin and inulin treatment

For mucin treatment, C57BL/6, C3H/HeOuJ or GF ASF-bearing C3H/HeN mice (male, 6~8 weeks old) were provided with drinking water with or without 3% mucin (Lee Biosolutions) starting 14 days before tumor inoculation. Water was changed every other day.

For inulin treatment, C57BL/6 or C3H/HeOuJ mice (male, 6~8 weeks old) received standard chow (TD. 94048, AIN-93M, Purified Diet, ENVIGO), standard chow enriched with long-chain inulin by substituting all sucrose and 5% of corn starch, or a modified chow (TD. 160256, Modified AIN-93M, Diet with 15% inulin, ENVIGO) starting 14 days before tumor inoculation. Chow was refreshed two times a week.

RNA extraction and qRT-PCR analysis

Total RNA was extracted from tumor samples using an RNeasy Fibrous Tissue Midi Kit (QIAGEN) or from cells using a High Capacity Reverse Transcriptase Kit (Invitrogen), according to the manufacturers' protocols. Purity and concentration of extracted RNA were determined by reading at 260 and 280 nm in a NanoDrop spectrophotometer (Thermo Fisher). qRT-PCR analysis was performed using a SYBR Green RT-PCR Kit (Invitrogen) on a Bio-Rad CFX Connect Real-Time system. Expression levels were normalized to 18S or Tubb5 levels. The sequence-specific primers used in this study are shown in Table S4.

BMDCs

BM cells were isolated from the tibiae and femurs of C57BL/6 mice and cultured in DMEM medium containing 10% FBS, 1% penicillin/streptomycin, and recombinant mouse GM-CSF (20 ng/mL; BioLegend) for 8 days at 37°C.

Isolation of IECs

A 10-cm section of mouse small intestine was opened longitudinally, minced, washed in 150 mM NaCl containing 1 mM DTT, and then resuspended in dissociation buffer (130 mM NaCl, 10 mM EDTA, 10 mM HEPES [pH 7.4], 10% FCS, and 1 mM DTT). The sections were incubated at 37°C for 30 min with vigorous shaking to release the IECs from the lamina propria. The IEC suspension was then carefully aspirated, centrifuged, and washed in ice-cold PBS.

Serum cytokine and chemokine detection

Serum cytokines and chemokines were quantified using the LEGENDplex™ mouse inflammation panel and mouse proinflammatory chemokine panel (BioLegend), respectively. All data were collected on an LSRFortessa and analyzed using LEGENDplex™ software (BioLegend).

In vivo antibody treatments

Mice were injected i.p. with 200 μg anti-PD-1 (clone RMP1-14) or rat IgG2a isotype control on days 7, 10, 13, and 16 after tumor inoculation. All mAbs for *in vivo* use were GoInVivo grade from BioLegend. CD4+ and CD8+ T cells were depleted by i.p. injection of 400 μg anti-mouse Thy1.2 (CD90.2, clone 30H12 from Bio X Cell) or rat IgG2b isotype control. Antibodies were injected two times a week starting on day 3 after tumor inoculation. The efficacy of depletion was assessed by FACS analysis of blood samples collected on day 8 after tumor inoculation.

In vivo OT-I T cell proliferation assay

CD8+ T cells were isolated from the spleens of naive OT-I CD45.1+ mice, labeled with CFSE, and injected i.v. into WT CD45.2+ C57BL/6 mice treated with or without mucin. After 24 h, the mice were injected s.c. with 1×10^6 B16-OVA melanoma cells. Seven days later, the spleen, tumor-draining lymph nodes, and non-draining lymph nodes were harvested and analyzed by flow cytometry. The proliferation of OT-1 CD8+ T cells was assessed by analysis of CFSE dilution within the population by gating on CD45.1+ CD8+ T cells.

CD8+ T cell enrichment

CD8+ T cells were enriched by negative selection (StemCell Technologies, Inc.) according to the manufacturer's instruction from spleens of C57BL/6 mice that were untreated or treated with mucin or inulin for 2 weeks. Briefly, the enrichment of mouse CD8+ naive T cells utilized a biotinylated antibody cocktail (Biotinylated CD4, CD11b, CD11C, CD19, CD24 and B220 antibodies) that were captured on streptavidin-coated magnetic beads. Pre-incubation of cells with the antibody cocktail-bound magnetic beads enriched the CD8+ T cells in solution. The purity of the enriched CD8+ T was confirmed by flow cytometry (> 95%). FACS analysis was performed using FlowJo software.

QUANTIFICATION AND STATISTICAL ANALYSIS

Unless otherwise noted, all data are shown as the mean ± s.e.m. Before statistical analysis, data were subjected to the Kolmogorov–Smirnov test to determine distribution. Variance similarity was tested using an *F* test for two groups and Bartlett's test for multiple groups. Two groups were compared using the two-tailed t test for parametric data or the Mann–Whitney *U* test for non-parametric data. Multiple groups were compared using one-way ANOVA with Tukey's, Dunnett's, or Bonferroni's correction for parametric data or using the Kruskal–Wallis test with Dunn's correction for non-parametric data. Tumor growth curves were analyzed using two-way ANOVA with Sidak's, Tukey's, or Bonferroni's correction for multiple comparisons. Statistical details of each experiment are indicated in the corresponding figure legends.

DATA AND CODE AVAILABILITY

The approach used to map microbiota taxa (Figures 5, 6, and S4) is detailed at: http://github.com/taolonglab/himap; BioRxiv 565572. The microbiome sequence data used for mapping the microbiota taxa have been deposited in NCI BioProject: PRJNA593851 https://www.ncbi.nlm.nih.gov/bioproject/PRJNA593851. The raw data of this manuscript was deposited online in the Mendeley archive https://data.mendeley.com/datasets/zrjr39f7mb/draft?a=28ed04b4-6d90-4eec-be59-c42e05589ade.